

PAIR PRODUCTION AND PULSAR CUTOFF IN MAGNETIZED NEUTRON STARS WITH NONDIPOLAR MAGNETIC GEOMETRY

JOHN J. BARNARD AND JONATHAN ARONS^{1,2}

Astronomy Department and Space Sciences Laboratory, University of California, Berkeley

Received 1981 June 18; accepted 1981 September 24

ABSTRACT

We construct models of the open field zone in pulsars in which we assume space-charge limited, time independent, electron flow from the surface of a conducting magnetized neutron star with dipolar and quadrupolar components to the magnetic field. We find that the radius of curvature of the field can be much less than in a pure dipole field and can be sufficient to account quantitatively for the cutoff line in the $P-\dot{P}$ diagram if systematic departures from our basic assumptions about the outer magnetosphere occur (such as decreasing the maximum radius of the last closed field line at small \dot{P}). We further investigate the effects on the cutoff line of three simple models of torque decay: ohmic decay of the dipolar magnetic field, magnetic field complication due to an MHD-secular instability suggested by Flowers and Ruderman, and alignment of the magnetic dipole axis with the rotation axis. We find qualitative dynamical differences from the pure dipole result (e.g., that potential drops at low altitude in the nondipolar field might result in self consistent particle acceleration even in the aligned rotator). We suggest possible observational consequences to the existence of higher order components to the field (e.g., differences in the polarization angle versus pulse longitude relation).

Subject headings: pulsars — stars:magnetic — stars:neutron

I. INTRODUCTION

Radio emission from pulsars implies the existence of quite large energy density radio waves within the emission region (brightness temperatures of up to 10^{30} K have been inferred from the observations; cf. Manchester and Taylor 1977). A collective emission mechanism is required; otherwise particle energies corresponding to the unphysically high temperature of $\sim 10^{30}$ K would be implied. Therefore, a plasma (either charge neutral or charge separated) of density sufficient to sustain collective behavior with oscillation frequencies in the radio range must exist somewhere within the vicinity of the pulsar. Goldreich (1969) and Sturrock (1970) suggested magnetic conversion of the γ -rays emitted by ultrarelativistic charged particles near the stellar surface as a likely source for a dense e^\pm plasma in the magnetosphere, in spite of the large surface gravity and low surface temperatures prevailing in neutron stars. The creation of pairs requires large accelerating electric fields near the stellar surface which in turn occur only if the magnetic field and rotation frequency are quite large. Isolated, magnetized neutron stars with long rotation periods and/or weak surface magnetic fields cannot create pairs. It is known (Lyne, Ritchings,

and Smith 1975; Manchester and Taylor 1977) that pulsar emission ceases for long rotation periods P , and small spin-down rates \dot{P} , a cutoff which may be due to the failure to create pairs (Sturrock 1970). The comparison of the theoretical criteria for pair creation to the observed form of the pulsar cutoff line in the $P-\dot{P}$ diagram affords an interesting test for pulsar models which have pair creation as a central element.

Sturrock's (1970) original estimate was roughly in accord with observations. However, his neglect of the effective corotation charge density led to an overestimation of the accelerating electric field. Arons and Scharlemann (1979, hereafter AS) and Arons (1981*b*) in a more complete model for relativistic flow above the polar caps found that in a pure dipole field with electrons freely available from the star, the cutoff period was 0.15 s for typical parameters. This is more than an order of magnitude less than the observed periods of the longest period pulsars. If particle emission from the surface is inhibited, pair creation in the resulting vacuum electric field may lead to pair creation in a pure dipole field at somewhat longer periods but still not at periods as long as those observed (Ruderman and Sutherland 1975, hereafter RS). RS do obtain a cutoff period ~ 1 s only after including magnetic fields with short radius of curvature near the surface, but without calculating the effect of changing the magnetic geometry on the accelerating electric field.

¹John Simon Guggenheim Memorial Foundation Fellow.

²Also Physics Department.

While the assumption of a pure dipole field is adequate for a qualitative understanding of pulsar spin-down (Goldreich, Pacini, and Rees 1972), the magnetic field at the surface could be much more complex. If the surface field contains contributions from multipoles of order l , the Poynting flux of angular momentum from the star is unaffected if

$$\beta_l \equiv \frac{B_l(r=R_*)}{B(r=R_*)} \ll \left(\frac{c}{R_*\Omega} \right)^{l-1}$$

$$= \left[5 \times 10^3 \left(\frac{P}{1 \text{ s}} \right) \left(\frac{10 \text{ km}}{R_*} \right) \right]^{l-1},$$

for $l \geq 2$. Here $B(r=R_*) \equiv 2\mu/R_*^3$ is the polar field of the dipole, μ is the dipole moment ($\sim 10^{30}$ cgs), B_l is the magnetic field of a centered l pole at its magnetic pole, R_* = stellar radius ~ 10 km, $\Omega_* = 2\pi/P$ is the angular frequency, and P = rotation period. If $\beta_l \gtrsim 1$ for one or more values of β_l , the radius of curvature of the surface magnetic field can be much smaller than that of the dipole field along polar field lines, where pairs are thought to be created.

The effect of having field structure with short radius of curvature, ρ , is threefold. Most directly, the energy ϵ of a typical curvature photon is increased since ϵ is proportional to $1/\rho$. Second, a strong component of the magnetic field perpendicular to the direction of motion of the photon is reached in a shorter distance, thus increasing the optical depth for pair creation in a field of fixed strength occupying a fixed volume. Third, the accelerating electric field (and thus photon energy) is increased since the curvature increases the rate at which the charge density departs from the corotation charge density, in models with space charge limited particle emission from the stellar surface (see eq. [8]).

All three effects tend to shorten the mean free path for γ -ray absorption and so increase the maximum period at which pair creation will be important. However, the inclusion of multipoles with $\beta_l > 1$ affects not only the curvature of the field but the size of the flux tube as well. Copious pair creation at long period requires the existence of large accelerating potentials (voltages ~ 1 TV) and intense magnetic fields ($B > 1$ TG) in the pair creation zone. Decreasing ρ well below ρ_{dipole} requires values of B in excess of B_{dipole} , which is roughly known by the observed torque on the star. The result is that the size of the open flux tube decreases with increasing B_{total} . This decreases the accelerating voltage, owing to the closeness of the conducting boundaries. Thus, achieving pair creation in rotating neutron stars with periods in excess of 1 second is nontrivial.

In this paper, we calculate the maximum period for pair creation when the magnetic field at the stellar surface is the superposition of a centered dipole and a centered, axisymmetric quadrupole whose axis is not parallel to the dipole axis, and we show that maximum periods in accord with observation can be obtained for a wide range of parameters. This choice of magnetic topology keeps the number of free parameters to a minimum. In addition, in some magnetic decay models, the magnetic field in older pulsars would have such a structure as the pulsar cutoff is approached. We do not calculate detailed models of the current flow and plasma production when P is substantially less than the cutoff period. In § II we outline our assumptions and method of solution for finding the maximum period for pair creation in an object of fixed dipole and quadrupole moments.

We present our specific models and results for the cutoff period in § III, showing the dependence on magnetic dipolar surface strength B_D , on the ratio of the polar quadrupole field to the polar dipole field, and on the orientation of the dipole moment and the quadrupole moment to the rotation axis. These results are applied to simple models of magnetic field decay and orientation in § IV. Observational consequences of higher order multipoles are presented in § V, with our final conclusions given in § VI.

II. ASSUMPTIONS AND METHOD OF SOLUTION

a) Assumptions

The basic assumptions are those of AS. We assume $\Omega \cdot B > 0$ over the whole polar cap, where the open flux tube intersects the stellar surface. The electrical forces then lead to extraction of electrons from the polar cap; these are assumed to be freely available from the dense stellar surface, so that $E \cdot B = 0$ at $r = R_*$ where E is the electric field. We assume this electrical extraction leads to current flow within the polar flux tube, and assume the necessary return currents are formed by flow across B in the outer magnetosphere. The flow is assumed to be steady in the corotating frame. A return current is assumed to form near the light cylinder where the increase in gyroradius and the longer lifetime against synchrotron radiation losses allow cross-field motion of the electrons, permitting a current to return to the star at lower magnetic colatitudes. The details of the return current are largely unexplored but are qualitatively discussed by Arons (1979, 1981a). For this discussion we simply postulate the existence of such a flow.

The boundary of the polar flux tube is assumed to be a good conductor, because of plasma drawn up from the stellar surface along closed field lines, or from pair creation by γ -rays emitted within the polar flux tube but absorbed in the closed zone, or because of plasma circulation and precipitation at high altitude, $r \sim c/\Omega_*$.

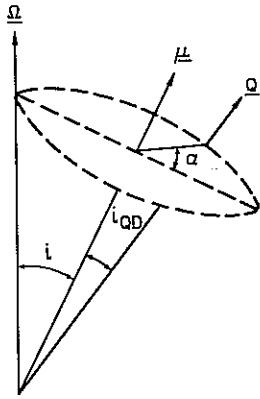


FIG. 1.—Magnetic field geometry. The magnetic dipole axis, μ , is inclined by angle, i , from the rotation axis Ω . The axis of symmetry of the quadrupole, Q , is tilted from the dipole axis by an angle, i_{QD} , and the (μ, Q) -plane is tilted by the dihedral angle α from the (Ω, μ) -plane.

The main change from the assumptions of AS is in the new magnetic geometry at low altitude. A small radius of curvature of the magnetic field occurs when a dipole field line far from the star is directed towards a pole of the quadrupole whose polarity is opposite to that of the dipole field, thus causing the field line to be redirected toward a region of the correct polarity near the stellar surface. We assume the presence of an axisymmetric magnetic quadrupole, Q , inclined by an angle i_{QD} from the dipole axis, μ . In turn μ is inclined by the obliquity i from the angular velocity Ω_* . The dihedral angle between the (μ, Q) -plane and the (μ, Ω_*) -plane is denoted by α , which is allowed to be arbitrary (see Fig. 1). The magnetic fields are specified by

$$\begin{aligned}
 B_{rD} &= B_D \left(\frac{R_*}{r} \right)^3 \cos \theta_D, \\
 B_{\theta D} &= \frac{1}{2} B_D \left(\frac{R_*}{r} \right)^3 \sin \theta_D, \\
 B_{rQ} &= \frac{1}{2} B_Q \left(\frac{R_*}{r} \right)^4 (3 \cos^2 \theta_Q - 1), \\
 B_{\theta Q} &= B_Q \left(\frac{R_*}{r} \right)^4 \cos \theta_Q \sin \theta_Q,
 \end{aligned} \tag{1}$$

where $(B_{rD}, B_{\theta D})$, $(B_{rQ}, B_{\theta Q})$ are the dipole and quadrupole field components referred to the dipole and quadrupole axes, respectively, with magnetic colatitudes θ_D and θ_Q . B_D and B_Q are the field strengths at the respective poles $\theta_D = 0, \theta_Q = 0$.

b) Geometry of the Polar, "Open" Flux Tube

A physical definition of the polar flux tube requires the construction of a global model of the magnetosphere, including the flow of conduction currents. Here we adopt a simple kinematic description, with parameters chosen in a manner similar to the description of Goldreich and Julian (1969). We assume that field lines of the dipole which pass exterior to a radius $R_A \equiv f_{pc} c / \Omega$ in the magnetic equator of the dipole are the field lines defining the polar flux tube. Here f_{pc} is a dimensionless number of order unity, in which we express our uncertainty about the details of the outer magnetosphere.

The field lines are determined by integrating the system:

$$\frac{dr}{B_r} = \frac{rd\theta_D}{B_\theta} = \frac{r \sin \theta_D d\phi_D}{B_\phi} \tag{2}$$

from $r = R_A, \theta_D = \pi/2$ inward to $r = R_*$. Here ϕ_D is the dipole magnetic azimuth. Note that the components of the total magnetic field appear in (2) even though dipole magnetic coordinates are used. Instead of integrating the full three-dimensional equations (2) for all values of ϕ_D , we simply integrated in the (μ, Q) plane within which the field lines are coplanar, and the system of differential equations reduces to:

$$\frac{dr}{d\theta_D} = r \frac{B_r}{B_\theta} \tag{3}$$

Integration of (3) yields two points on the intersection of the polar flux tube with the stellar surface. From the reflection symmetry of the dipole and quadrupole field across the (μ, Q) -plane we know that a good approximation of the cross sectional shape of the polar flux tubes will be an ellipse with one of the principle axes in the (μ, Q) -plane. One semiaxis of the ellipse $\Delta x(r)$ is determined by numerical integration of (3). The other semiaxis is determined by flux conservation. To first order in R_*/R_A , the magnetic flux of the polar flux tube is the dipolar flux crossing outside R_A :

$$F = \frac{2\pi\mu}{R_A} = \pi B_D R_*^2 \left(\frac{R_*}{R_A} \right) \tag{4}$$

At fixed radius $r \ll R_A$, the magnetic field is approximately constant over the area of the tube. Therefore the other semiaxis is:

$$\Delta y(r) = \frac{R_*}{R_A} \frac{B_D}{B(r)} \frac{R_*}{\Delta x(r)} R_* \tag{5}$$

Some examples of flux tube shapes are shown in Figure 2.

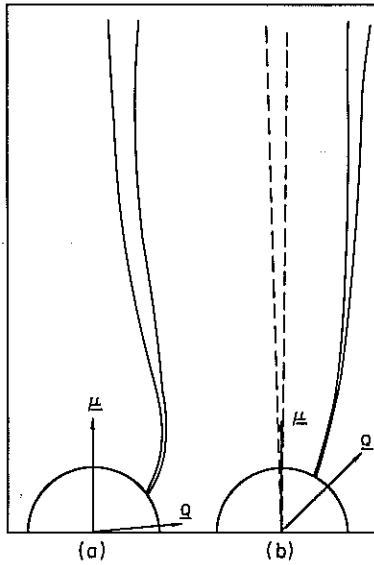


FIG. 2.—Examples of polar flux tubes. *Solid lines*, two examples of flow tubes with a nonzero magnetic quadrupole moment. (a) $i_{\text{QD}}=83^\circ$, (b) $i_{\text{QD}}=45^\circ$. In both (a) and (b) $\beta=4$ and $R\Omega/c=5\times 10^{-3}$. *Dashed Lines in (b)*: Flow tube of pure dipole field, with same period. Note that the curvature of the dipole field is imperceptible on this scale although clearly seen from the curves in which $\beta\neq 0$.

In actually solving (3) we begin at $r=R_A$, $\theta_D=\pi/2$, with the magnetic field given as a dipole plus a small perturbing component from the quadrupole. This allows an analytic solution for the field lines in the (μ, θ) -planes, valid when $r\gg\beta R_*$, if $\beta\gtrsim 1$ (Here $\beta\equiv B_Q/B_D$). Near the star, this analytic solution is continued to the surface by numerical integration. (The analytic solution is presented in Appendix B.)

c) Poisson Equation and Accelerating Potential

Because the system is steady in the corotating frame, there exists a potential Φ such that the electric field $E=-c^{-1}(\Omega_*\times r)\times B-\nabla\Phi$ (Backus 1956; Mestel 1971). From Poisson's equation, Φ satisfies (6):

$$-\nabla^2\Phi=4\pi(\eta-\eta_R), \quad (6)$$

with η =charge density and

$$\eta_R=\frac{-\Omega\cdot B}{2\pi c}+0\left(\frac{r\Omega}{c}\cdot\frac{\Omega\cdot B}{2\pi c}\right); \quad (7)$$

η_R is the charge density such that $\Phi=0$, and the electric field vanishes in the corotating frame (Goldreich and Julian 1969).

We consider geometries such that $\Omega\cdot B>0$ at the stellar surface. Therefore, equation (7) shows that only electrons are electrically extracted from the star. When the field is favorably curved at the stellar surface, par-

ticles become relativistic in a distance $\sim c/\omega_p\equiv c(m_e/4\pi e|\eta_R(R_*)|)^{1/2}$ which is much less than a polar cap width (Michel 1975; Fawley, Arons, and Scharlemann 1977, hereafter FAS). So, with speed $\approx c$, continuity of flow and conservation of flux yield $\eta\propto B$. The requirement that the flow be space-charge limited ($E\cdot B=0$ at the stellar surface) yields: $\eta=\eta_R(R_*)(B/B_*)$ +small corrections. Also we assume $B_*=B(r=R_*)$ =constant across the open flux tube. Then Poisson's equation is:

$$-\nabla^2\Phi=4\pi\eta_*\left(\frac{B}{B_*}\right)\left(1-\frac{\cos\xi}{\cos\xi_*}\right). \quad (8)$$

Here $\xi=\angle[B(r),\Omega_*]$ and $\xi_*=\xi(r=R_*)$ on the field line which passes through the point r . If the field lines are straight, $\xi_*=\xi$, Φ =constant (Tademaru 1974) and no acceleration occurs. If $\xi<\xi_*$ and if $\cos\xi>\cos\xi_*$, the flux tube bends toward the axis of rotation while the field lines point from the axis, and the flow of charge along B fails to supply the charge density required to keep $\Phi=0$ at any point $r>R_*$. This portion of the magnetosphere is then starved of charge, and the "starvation" electric field (Arons 1981a) accelerates the electrons to very high energy. In the geometries of interest here, the curvature of the flux tube as a whole is much greater than the curvature of the field line due to the increase of the cross section with altitude, in contrast to the dipolar flux tube considered in previous work. Then $\xi(r)\approx\xi(r)$ and $\eta-\eta_R$ is almost constant across a cross section of the flux tube at a given radius.

The remaining boundary conditions are that $\Phi=0$ on the boundary of the flux tube. When pair creation is important, a further boundary condition $E\cdot B/B\rightarrow 0$ as $r\rightarrow R+h$ is also needed (AS; Arons 1981b). Here $R+h$ is the altitude of the pair formation front. The former condition represents the hypothesis that the closed zone of the magnetosphere is unable to support the large voltage drops present along polar field lines, because of a denser trapped plasma. Since the polar flux tube is long and narrow, we can now find a simple solution by noting that $\nabla_\perp^2\Phi\gg\nabla_\parallel^2\Phi$. Then to an excellent approximation the potential problem is the same as that of a grounded, infinitely long elliptical tube with constant charge density, $\eta-\eta_R$, in the interior; the height above the stellar surface, $r-R_*$, appears only as a parameter. The solution to this problem is found to be:

$$\Phi=\frac{2\pi[\eta(r)-\eta_R(r)]}{\Delta x^2+\Delta y^2}(\Delta x^2\Delta y^2-x^2\Delta y^2-y^2\Delta x^2)$$

or

$$\Phi=\frac{\Omega_*F}{\pi c}(\cos\xi-\cos\xi_*)\frac{\Delta y/\Delta x}{1+\Delta y^2/\Delta x^2}\times\left(1-\frac{x^2}{\Delta x^2}-\frac{y^2}{\Delta y^2}\right). \quad (9)$$

Equation (9) is valid when "end effects" are unimportant, i.e., when $\Delta x, \Delta y \ll r - R_*, R_* + h - r$. Here x and y are the Cartesian coordinates of a field point, with origin of coordinates at the center of the ellipse, x -axis in the (μ, Q) -plane and y -axis perpendicular to this plane, $\Delta x(r)$ and $\Delta y(r)$ are the previously determined semiaxes, and F is the magnetic flux in the polar flux tube.

It should be noted that (9) is not strictly correct in a purely dipole flux tube, since in this case the curvature of the field lines is dominated by the divergence of the field lines from the magnetic axis rather than the curvature of the whole flow tube. Nevertheless, the flow in the dipole zone has the same qualitative properties exhibited by (9).

The basic hypothesis behind (9) is that strong acceleration occurs in a distance $r \sim \beta R_*$ from the star and that further changes in the potential do not reduce the potential to values below $\Phi(R_*)$. From (9) we see that potential increases when the flux tube curves toward the rotation axis while directed away from the rotation axis or if the flux tube curves away from the rotation axis while directed toward it, both situations ensuring that $\cos \zeta - \cos \zeta_*$ increases monotonically. The minimum requirement of unidirectional electron flow is that $\Phi(R_A) > \Phi(R_*)$ along a field line from the surface to $r \sim R_A$. Figure 3 shows those models for which the central field line of the flux tube does have "favorable" curvature for strong acceleration, for fixed i_{QD} , varying β and for fixed β varying i_{QD} . Note that the graphs include models in which the dipolar field is unfavorable at high altitudes ($r \leq c/\Omega$), even though along the central field line each model has a nonzero potential increase, for all models. Note also that $i=0$ (aligned rotator), in some circumstances, can have finite particle acceleration, a result of the low altitude potential difference being greater than the loss of energy occurring in the unfavorably curved dipole zone, in contrast to the inconsistency of such flow in the purely dipolar case (Scharlemann, Arons, and Fawley 1978, hereafter SAF). Actually, when $r \sim c/\Omega$, the question of favorable curvature becomes moot since η_R is no longer given by $(-\Omega \cdot B/2\pi c)$ but rather is a more complicated function of position (e.g., see FAS). Since steady flow can exist along the central field line, however, the model will be self-consistent for some bundle of field lines along the central one. On field lines where pairs are created copiously at low altitudes, high-altitude curvature is less important since the potential drop is limited by the creation of pairs, not the high-altitude curvature; however, high-altitude curvature remains the controlling factor in the "slot gap" surrounding the pair plasma (Arons 1981a).

Thus, at least half of the configurations can maintain the flow while the other half may not, and most likely form an electrically trapped atmosphere with little or no

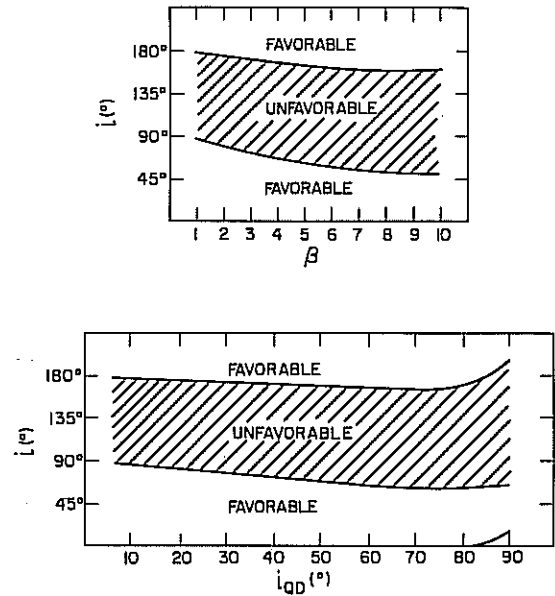


FIG. 3.—Favorable curvature. Two examples of those areas in the model's parameter space which give rise to favorable curvature along the central field line for $r < c/\Omega$. Shown are: (a) (top) i versus β , with $i_{QD} = 45^\circ$ and $\alpha = 0$; (b) (bottom) i versus i_{QD} with $\beta = 4$ and $\alpha = 0$.

current flow (SAF), a situation locally akin to possible states of the aligned rotator (Jackson 1976; Michel and Pellat 1981). Acceleration above the trapped zones is possible if favorable curvature occurs at higher altitudes.

Note that these models produce potentials which are nonmonotonic even though the net change in potential is positive along a field line. Rylov (1979) suggests that if the potential has a "hump" in it, as can be true for this class of models, a population of nonstreaming electrons will be trapped until the hump is removed and the potential is monotonic. Although this is certainly an alternative self-consistent solution, we find it to be unphysical, since, as is pointed out by Rylov, the plasma distribution is then highly two-stream unstable. The cold electrons are quickly entrained by the beam, and so are removed rapidly, requiring a replenishment rate sufficient to maintain the static electrons. But since the potential increase to the "humps" ($\sim \text{TeV}$) is much greater than the initial spread of energies at the surface ($\sim \text{keV}$), no surface particles will be trapped in the hump, and the boundary conditions that $\Phi = 0$ along the flux tube eliminate the possibility of replenishment from the closed zone. We thus argue that the nonmonotonic potentials are not unstable to monotonic potentials suggested by Rylov. However, as noted above, trapped particle zones are indeed relevant when the geometry is sufficiently complicated that zeros occur in the potential when calculated on the basis of a flowing plasma.

d) *Pair Creation*

When the surface magnetic field is $\sim 10^{12}$ gauss, the potential (9) can easily have magnitudes \sim TV or greater. Gamma-rays which are emitted by the TeV electrons moving on the curved field lines can create pairs through magnetic conversion of the photons. Processes other than curvature emission and magnetic conversion are not important (Cheng and Ruderman 1977; FAS; Fawley 1978), especially in the long period objects of interest here. The characteristic photon energy is:

$$\epsilon = \frac{3}{2} \frac{\lambda_c}{\rho} \left(\frac{e\Phi}{mc^2} \right)^3 mc^2, \quad (10)$$

where $\lambda_c = \hbar/m_e c = 3 \times 10^{-11}$ cm and the radius of curvature of a field line is

$$\rho = \frac{[r^2 + (dr/d\theta)^2]^{3/2}}{[r^2 + 2(dr/d\theta)^2 - r(d^2r/d\theta^2)]}. \quad (11)$$

Here $dr/d\theta$ is given by (3) and $d^2r/d\theta^2$ is calculated from (1) and (3) after (1) is combined in the (μ, Q) -plane to obtain an expression for B in dipole coordinates.

Once we know the energy of a gamma ray at any emission point, r_e . We then calculate the optical depth along a straight ray parallel to $B(r_e)$ and extend from r_e to infinity. The opacity for magnetic conversion is

$$\kappa(r, \epsilon, B_\perp) \approx 0.23 \frac{\alpha_f B_\perp}{\lambda_c B_q} \exp\left(\frac{-8}{3} \frac{B_q}{B_\perp} \frac{m_e c^2}{\epsilon}\right). \quad (12)$$

(Erber 1966; Tsai and Erber 1974), where α_f is the fine structure constant, $B_\perp(r) = B(r) \sin \Psi$ is the component of the magnetic field perpendicular to the ray at the point r , Ψ is the pitch angle of the photon with respect to $B(r)$, and $B_q = m_e c^2 / eh = 4.4 \times 10^{13}$ gauss. The magnetic geometry and spatial location of the emission point are determined by the parameters P (observable), B_D (estimated from simple spin-down theory), B_Q , i , i_{QD} , and α (all inaccessible to direct observation). Since the photons are emitted parallel to $B(r_e) \equiv B_e$, B_\perp along a ray is simply given by $B_\perp = |B_e \times B(l)| / B_e$, where $B(l)$ is the magnetic field on the ray at a distance l from the emission point. The optical depth for photons of energy ϵ is $\tau = \int \kappa dl$. For the geometries considered, τ must be evaluated numerically.

e) *Method of Determining the Maximum Period of Pair Creation*

In order to determine the maximum optical depth in a given magnetic geometry, we first integrate the field line

equations from $r = R_A$ to the surface for the two field lines which form the ends of the polar flux tube in the (μ, Q) -plane, and use the total open flux to find the shape of the open flux tube. The corotation charge density η_{R*} is then determined as is the charge density of the electron beam, $\eta = \eta_{R*}(B/B_*)$. We then reintegrate the field lines outward along the flux tube, keeping track of the dimensions of the tube as well as the location of the center of the tube where the potential is maximum. The maximum γ -ray energy is calculated at each point as is the radius of curvature of the magnetic field.

The optical depth for a photon emitted at r_e is then calculated by integrating the opacity (12) for a photon of energy $\epsilon[\Phi(r_e), \rho(r_e)]$ along the ray which is tangent to $B(r_e)$ and begins at r_e . The photon, traveling a nearly straight path in the corotating frame, sees increasing B_\perp as the field curves away from the original photon direction. However, owing to the decrease of B with increasing height, the opacity reaches a maximum, then rapidly declines. The optical depth increases to a maximum value for each emission point of interest. If $\tau_{\max}(r_e)$ is reached inside the polar flux tube, and $\tau_{\max}(r_e) < 1$, exponentially few pairs are formed, and the creation of pairs is said to be "opacity bounded." If τ_{\max} is reached beyond the point where the photon crosses the closed zone, and if $\tau(r_e, s) < 1$ everywhere within the polar flux tube, then pair creation is said to be "geometry bounded," since production of pairs in the closed zone is unlikely to contribute to radio emission in the open zone. In a pulsar which does create pairs in the open flux tube the additional formation of pairs in the closed zone by photons of energy $\epsilon < \epsilon_c$ in the curvature spectrum is an important contribution to plasma in the closed zone and so helps justify our use of conductive boundary conditions for the polar flux tube.

In a given magnetic geometry we find the maximum period for pair creation by finding the period P_m such that for $P > P_m$ all emission points along the central field line of the polar flux tube have $\tau_{\max}(r_e) < 1$, or are geometry bounded. For $P < P_m$, there is at least one point r_e where $\tau_{\max}(r_e) > 1$ inside the polar flux tube. The exponential form of the opacity assures us that pair creation will be copious when $P < P_m$, and by assumption results in radio emitting pulsars. For $P > P_m$ the number of pairs per primary electron is exponentially small, leading (perhaps) to pure γ -ray pulsars (Fawley 1978; SAF; Kennel 1979; Scharlemann 1979; Harding 1981). P_m is determined as a function of B_D , B_Q , and the various angles by varying these parameters over the range of interest.

III. RESULTS WITH GENERAL OBLIQUITY

The simplest geometry considered was obtained when μ and Q are aligned ($i_{QD} = 0$). The resulting axial symmetry allows an analytic solution, which is presented in

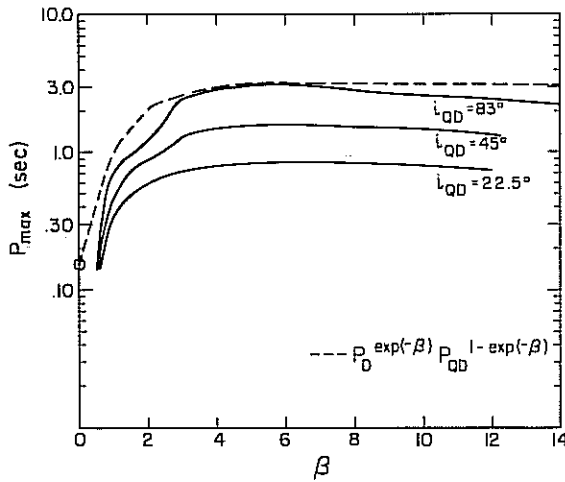


FIG. 4.— P_{\max} vs. β . The maximum period for pair creation is given as a function of β for three values of i_{QD} with $i (= 45^\circ)$, $\alpha (= 0)$, and $B_0 (= 4.4 \times 10^{12}$ gauss) held constant. The dotted line is our analytic approximation which is applied in the text to evolutionary scenarios. The circle gives the result of AS for a pure dipole field.

Appendix A. When the dipole is tipped with respect to the quadrupole, axial symmetry with respect to the magnetic axis is lost, so the numerical approach outlined in § II applies. For a given geometry (i_{QD} , i , and α), dipole field strengths B_D , and field strength ratio β , we determine the maximum period such that $\tau = 1$ at one point along the central ray of the flux tube and $\tau < 1$ everywhere else. Our results for P_{\max} are presented in Figure 4. The most important parameters are i_{QD} and β ,

for these determine ρ while α and i enter into the problem only through $\Omega \cdot B$ in η_R . The quantity ρ_* is plotted as a function of i_{QD} and β in Figure 5a. Also the dipole latitude of the polar cap is shown in Figure 5b. In these general geometries, the full requirement for pair creation in long-period pulsars ($\rho \ll \rho_{\text{dipole}}$ with potentials and field strengths comparable to the dipolar values) are achieved. It can be seen that for small values of β , P_{\max} approaches the dipole value found by AS, when the radius of curvature of the twisting flow tube in the perturbed dipole case is on the order of the radius of curvature of the diverging flow tube of the pure dipole case. The largest value of P_{\max} is found for $\beta \sim 6$; however, once $\beta > 3$, the maximum period is quite insensitive to β . This result is a consequence of several competing effects. As β is increased to values greatly exceeding unity, the local geometry as $r \approx R_*$ reverts to an approximately pure quadrupole. From flux conservation, the area of the flow tube decreases in proportion to $1/\beta$. In addition, ρ increases in proportion to β since ρ is proportional to the radius at which the quadrupole merges with the dipole. These effects reduce Φ (which is proportional to the area of the flux tube and decreases when ρ increases since $\eta - \eta_R$ varies inversely with ρ). They also reduce ϵ , which is proportional to $\rho^{-1} \Phi^3$, and reduce the pitch angle $\Psi \propto \rho^{-1}$ for a fixed distance of travel, thus reducing the overall opacity. However, as β increases, B increases linearly with β so that B_\perp remains fixed, and Φ is increased simply because $\eta - \eta_R$ is proportional to $B \propto \beta$. The net effect is to yield a P_{\max} largely independent of β as long as $\beta > 3$.

The effect of varying i_{QD} is also straightforward. The quadrupole, being axisymmetric, has a belllike zone of

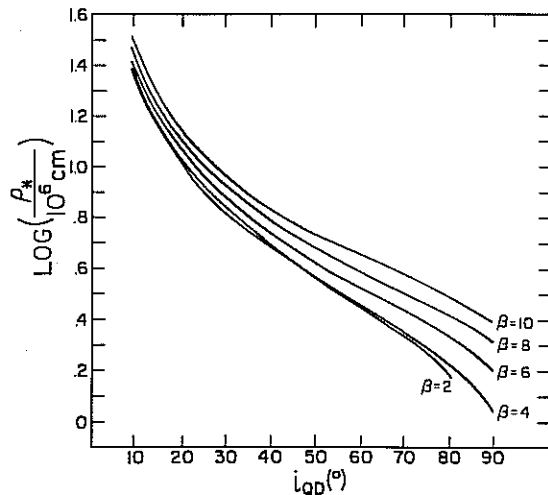


FIG. 5a

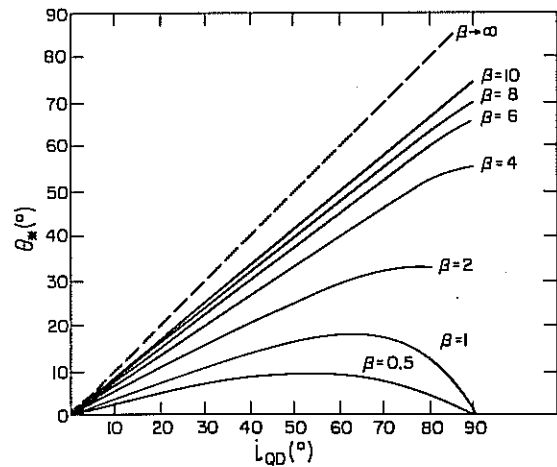


FIG. 5b

FIG. 5.—(a) Radius of curvature of central field line at stellar surface. Note that ρ_* increases as β increases and as i_{QD} decreases. For $\beta < 2$, ρ_* increases as β decreases. (b) Magnetic colatitude of central field line at stellar surface, for various values of β , plotted as a function of i_{QD} .

flux emerging from the star in addition to two poles similar in character to the dipolar poles. When $i_{QD}=0$, the dipole field in one hemisphere merges into the equatorial belt region, described in Appendix A. The efficiency for pair creation is reduced because of the narrow striplike character of the zone. (The other hemisphere has quadrupole and dipole fields aligned at the surface and hardly differs from the dipole case.) When $i_{QD} \sim 1$, however, the dipolar flux tube is rerouted by an angle $\sim i_{QD}$ when $\beta > 1$ while still preserving its tubelike character, so that small ρ is achieved without sacrificing the large magnitude of the potential and opacity achieved in the dipole case.

To determine their effect on P_{\max} , each of the quantities $(\Delta\theta_{\text{cap}}/\Delta\theta_{\text{GEOM}})$, $(\bar{\epsilon}/\epsilon_{\text{crit}})$, B_D , and R were varied independently. Here $(\Delta\theta_{\text{cap}}/\Delta\theta_{\text{GEOM}})$ is the ratio of the actual cap width to the width of the cap found by tracing the field line passing through the magnetic equator at $\theta_d = \pi/2$; $\bar{\epsilon}/\epsilon_{\text{crit}}$ is the ratio of the actual photon energy to twice the peak of the curvature spectrum. The parameter ϵ_{crit} was defined to be at twice the energy of the peak in the curvature spectrum because previous work (AS; Arons 1981b) showed that the pair creation rate is maximum at their energy, owing to the higher energy albeit lower emission rate than the actual peak in the curvature spectrum.

Combining these effects into a single relation yields:

$$P_{\max} \propto \left(\frac{\Delta\theta_{\text{cap}}}{\Delta\theta_{\text{GEOM}}} \right)^{1.0} \left(\frac{\bar{\epsilon}}{\epsilon_{\text{crit}}} \right)^{0.04} \left(\frac{B_D}{4.4 \times 10^{12} \text{ G}} \right)^{0.68} \times \left(\frac{R_*}{10 \text{ km}} \right)^{1.2}. \quad (13)$$

Although Figure 4 is the most accurate representation of our results, for the evolutionary applications which follow, P_{\max} can be represented approximately by:

$$P_{\max} = P_{QD}^{1-a} P_D^a \left(\frac{\Delta\theta_{\text{cap}}}{\Delta\theta_{\text{GEOM}}} \right)^{1.0} \left(\frac{\bar{\epsilon}}{\epsilon_{\text{crit}}} \right)^{0.04} \times \left(\frac{B_D}{4.4 \times 10^{12} \text{ G}} \right)^{0.68} \left(\frac{R_*}{10 \text{ km}} \right)^{1.2} \text{ s}. \quad (14)$$

Here $P_D \approx 0.15 \text{ s}$, $P_{QD} \leq 3.08 \text{ s}$, and $a = e^{-\beta}$. P_{QD} depends on i_{QD} , α , and i and is graphed as function of the parameters in Figure 6. P_{QD} was found numerically to be a linear function of i_{QD} . For example, when $\alpha=0$, $i=45^\circ$, and $i_{QD} \leq 81^\circ$, P_{QD} satisfies: $P_{QD} = 3.08(i_{QD}/81^\circ) \text{ s}$. Although in AS, $P_D \propto (\sin i)^6 / B_D^{3/17}$, we have neglected the dependence of P_D on $\sin i$ and B_D in (14), since it is applied to cut off in the real P - P diagram only when $a \approx 0$ (§ IV).

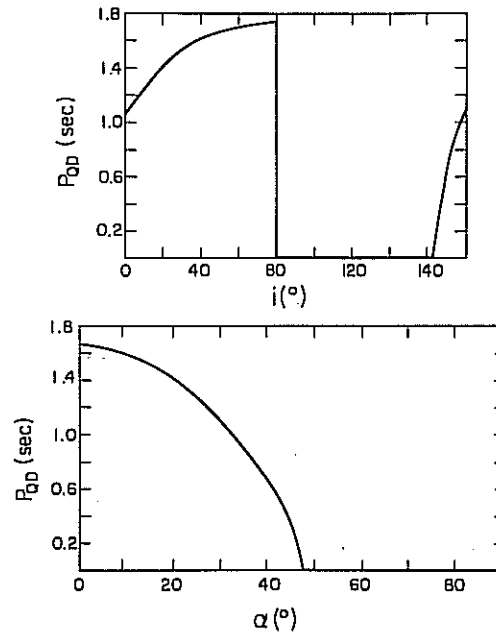


FIG. 6.—Examples of P_{QD} plotted as a function of model parameters. (a) (top) P_{QD} vs. i , ($\alpha=0$ and $i_{QD}=45^\circ$) and (b) (bottom) P_{QD} vs. α ($i=45^\circ$, $i_{QD}=45^\circ$). The sharp drop in P_{QD} in (a) and the zero value of P_{QD} in (a) and (b) are due to the changeover from favorable to unfavorable curvature. In some cases with unfavorable curvature at the surface, trapped particle zones may occur at the stellar surface, with acceleration occurring higher up, yielding nonzero P_{\max} in the regions where our P_{QD} formally indicates $P_{\max}=0$. The sharp boundaries between $P_{QD}=0$ and $P_{QD} \neq 0$ in the figure is thus due in part to our requirement of favorable curvature at the surface.

Thus far, we have assumed the simple space-charge limited flow of electrons from the surface is the basic source of γ -ray emission and therefore of pairs. This may seem restrictive, given the plethora of alternative models based on ion zone physics (RS; Cheng and Ruderman 1977, 1980; Jones 1978, 1979, 1980) proposed in the literature. However, our conclusions are more general. In all of these models including our own, pair creation cutoff occurs basically because a threshold voltage for pair creation $\Phi_0(B_{\text{surface}}, P) \sim 10^{12} \text{ V}$ (with Φ_0 almost independent of B_s, P) becomes smaller than the maximum voltage available on open field lines (cf. eq. [9]):

$$\Phi_{\max} \approx \frac{1}{f_{\text{pc}}} \left(\frac{R_* \Omega}{c} \right)^2 B_D R_* \cos i. \quad (15)$$

The main effect of the short radii of curvature in the models discussed here is to allow voltages of this magnitude to be reached in the low altitude high opacity region $r \leq 2\beta R_*$, even with free emission of particles

from the surface. The resulting P_{\max} can be written:

$$P_{\max} = 7.6 f_{pc}^{-1/2} \left(\frac{\Phi_0}{10^{12} \text{ V}} \right)^{-1/2} \left(\frac{B_D}{4.4 \times 10^{12} \text{ G}} \right)^{1/2} \times (\cos i)^{1/2} \text{ s.} \quad (16)$$

Note that the exponent of B_D in (16) is $\frac{1}{2}$, compared to 0.68 for the present paper and similar values in other theories. The departure from $\frac{1}{2}$ indicates the extent to which the potential systematically departs from the assumed constant potential drop of 10^{12} V. (For a comparison with other theories, cf. eq. [18] and Table 1.)

IV. THE RELATION OF P_{\max} TO THE OBSERVED CUTOFF IN THE $P-\dot{P}$ DIAGRAM

We assume that the apparent sharp absence of pulsars in the $P-\dot{P}$ diagram (observed by Lyne, Ritchings, and Smith 1975 to occur if $\dot{P} < \sim 4.6 \times 10^{-17} P^3$, where \dot{P} is measured in seconds s^{-1}) is due to the cessation of pair creation. If this assumption is true, a number of factors affect the location of the cutoff line in the $P-\dot{P}$ diagram.

1. Evolutionary history of the surface field complexity, assumed in this analysis to be composed only of the quadrupole and dipole components.

2. Evolutionary history of the strength and inclination of the dipole field.

3. Departure of the field near the light cylinder from that of a rapidly rotating magnetic dipole.

The first factor connects P_{\max} to the age of a pulsar, while the second factor connects the torque (and so \dot{P}) to age. The third factor enters in two ways: Distortions near the light cylinder may cause the last closed field line to be interior to R_L ($\equiv c/\Omega$) which we have defined before as R_A . On the other hand, if the rotational energy loss, \dot{E} , is dominated by the electromagnetic torque, then the energy loss is just the integral of the Poynting flux over a surface enclosing the star which can be

estimated to be (Goldreich, Pacini, and Rees 1971; Arons 1981c)

$$\dot{E} \sim cR_T^2 B_T^2 \sim c\mu^2/R_T^4, \quad (17)$$

where R_T is the radius at which B_ϕ and B_r are equal and B_T is the magnitude of B at this radius. R_T and R_A may in fact be equal, but for the moment we maintain their generality.

Since there are uncertainties in our knowledge in each of the three factors affecting the cutoff line, we will simply identify some plausible hypotheses concerning magnetic field evolution and indicate the effect each hypothesis has on the cutoff line, separately.

To be specific, we consider the following four different scenarios:

A) R_A and $R_T \neq R_L$.—The surface and dipole fields are assumed static in time, although we allow for the possibility of plasma-induced modifications to the outer magnetosphere (Roberts and Sturrock 1972; RS).

B) *Field decay*.—We assume the dipole and quadrupole moments suffer Cowling mode decay (suggested by Gunn and Ostriker 1969), such that $B_D = B_{D0} e^{-\gamma_D t}$ and $B_Q = B_{Q0} e^{-\gamma_Q t}$, where $\gamma_Q = 3.33 \gamma_D$ (Lamb 1883) and 0 indicates initial values.

C) *Field complication*.—We assume, following a suggestion of Flowers and Ruderman (1977), that due to the interaction between decay of poloidal currents in the resistive crust with MHD motions in the highly conducting core, the surface fields tend to become more complex with time while the magnitude of the surface fields remains fairly constant. We model this by assuming $B_D = B_{D0} e^{-\gamma t}$ while $B_Q = B_{D0}(1 - e^{-\gamma t})$. Note that we have assumed B_D and B_Q change at the same rate, and that γ is related to the crustal decay time

$$\sim \frac{c^2}{4\pi\sigma_{\text{crust}}} (\Delta R^2),$$

TABLE 1
PARAMETERS FOR P_{\max} IN POLAR CAP, PAIR PRODUCTION MODELS

| Reference | n | l | p | $A_1 \cdot (4.4 \times 10^{12} \text{ gauss})^n$ (s) | Remarks |
|------------------------------|------|-----|------|--|---|
| Sturrock 1971 | 0.57 | ... | ... | $2.2 (R/10^6 \text{ cm})^{9/7}$ | |
| RS 1975 | 0.62 | ... | ... | $4.2 (R/10^6 \text{ cm})^{21/13} (\rho/10^6 \text{ cm})^{-4/13}$ | |
| Cheng and Ruderman 1977. . . | 0.71 | ... | ... | $3.9 (\rho/10^6 \text{ cm})^{-4/7}$ | Curvature radiation produced |
| | 0.60 | ... | ... | $1.2 (f_{RS}/.01)^{-1/5}$ | Lorentz-boosted pair production (f_{RS} = fraction of polar cap filled by spark) |
| AS 1979 | 0.53 | .4 | -.60 | $1.5 (R/10^6 \text{ cm})^{19/15} (\rho/10^6 \text{ cm})^{-2/15}$ | Multipole estimate |
| | 0.47 | .35 | -.65 | $0.17 (R/10^6 \text{ cm})^{21/17}$ | Pure dipole |
| Jones 1980 | 0.50 | ... | ... | $3.1 (R/10^6 \text{ cm})^{3/2}$ | |
| This work 1982 | 0.68 | ... | ... | $3.0 (R/10^6 \text{ cm})^{1.2}$ | |

$\sigma_{\text{crust}} = \text{crustal conductivity} = 10^{23} \sigma_{23} \text{ s}^{-1}$, so that $\gamma^{-1} \sim 2 \times 10^5 \sigma_{23} (\Delta R / 1 \text{ km})^2$ years. It is possible to have $\sigma_{23} \ll 1$ if one accounts for inhomogeneities in the Coulomb lattice.

D) *Dipole alignment*.—We assume constant B_D, B_Q, α, i_{QD} , but assume that i obeys $\sin i = \sin i_0 e^{-t/\tau}$, where i_0 is the original value of i . Dipole alignment implies decay of the torque if the aligned rotator is electromagnetically quiescent (e.g., SAF 1978; Michel and Pellat 1981), in contrast to the scenario of Goldreich and Julian (1969).

Scenarios B, C, and D all imply decay of the torque as the star ages and crosses the $P-\dot{P}$ diagram. On observational grounds this statement is well founded for four reasons:

1. A much smaller range in initial magnetic field strengths is required to match the observed range in \dot{P} (Lyne, Ritchings, and Smith 1975 [LRS]).

2. The lower left edge to the distribution of pulsars is best fitted by a decaying torque model (LRS; Fujimura and Kennel 1979).

3. The number of pulsars per unit age interval is approximately constant for early ages only if torque decays with $\tau \sim 10^6$ years (Fujimura and Kennel 1979; Phinney and Blandford 1981).

4. The existence of many pulsars with apparent ages (P/\dot{P}) of 10^7 to 10^8 years contradicts the observed kinematic age of pulsars of $\sim 10^6$ years (based on velocities deduced from proper motions and distances deduced from dispersion measures) (Gunn and Ostriker 1970; Manchester and Taylor 1977).

Although the original motivation for appealing to torque decay (absence of large period pulsars) (Gunn and Ostriker 1969) is removed, the evidence is still strong that the torque nevertheless decays. Each of the theoretical mechanisms for torque decay, however, has its problems. The Cowling mode decay (Gunn and Ostriker 1969) may be true for the crust; but if the field is rooted deep in the core, the conductivity is expected to be higher, since the core is likely to be superconducting (Baym, Pethick, and Sutherland 1971). Flowers and Ruderman (1977), however, have observed that the fluidity of the core implies that the dipole field is MHD unstable to formation of higher order multiple components, thereby reducing the total external magnetic energy (see also Markey and Tayler 1973 for quantitative theory). However, they also realized that a toroidal magnetic field may exist which prevents the instability, and that the toroidal field requires poloidal currents which may pass through the crust. Ohmic decay of these currents on the crustal decay time could then result in decay of the dipole on the same time scale, converting the dipole field into quadrupole and higher order components. As yet, no quantitative calculations of this effect have been carried out. Alignment has been theoretically described by Michel and Goldwire (1970) and

Davis and Goldstein (1970) using a rigid conducting magnetized sphere in vacuum as a model for the neutron star. In this model, alignment occurs exponentially on a time scale determined by the initial value of $\Omega \cos i$. Goldreich (1970) and Macy (1974) have shown, however, that the ratio of poloidal to toroidal interior field strengths plays an important role, making alignment for most pulsars more problematic. Jones (1976) also considered alignment, and assumed that interior poloidal fields are dominant and are the dominant factor which determines the departure of the moment of inertia from that of a sphere. Goldreich and Julian (1969) suggested that torques associated with conduction current flow in the aligned rotator may be comparable to those of the vacuum rotator. If true, alignment does not imply substantial torque decay. However, recent work (Okamoto 1974; Holloway 1975; Jackson 1976; SAF; Michel 1979; Michel and Pellat 1981) have revealed a host of difficulties with the view that aligned rotators are indeed similar to oblique rotators in their gross spin-down properties. Indeed, it has been argued (SAF; Arons 1979, 1981a; Michel and Pellat 1981) the aligned cases and sufficiently oblique cases may be intrinsically different. We assume this latter point of view here, and go further to assume the torque is proportional to $\sin^2 i$, as in the vacuum case.

For most polar-cap pair-creation models, including those in this paper, we may write, in general,

$$P_{\text{crit}} = A_1 [\beta(t)] B_D^n(t) f_{\text{pc}}^p \sin^l i(t) \quad (18)$$

and

$$B_D^2(t) \sin^2 i(t) = A_2 P \dot{P} f_T^4, \quad (19)$$

where $A_1, p, n, l, f_{\text{pc}} \equiv R_A/R_L, f_T \equiv R_T/R_L$ are determined by the model and scenario selected and are summarized for various models in Table 1. Note that (19) is identical to (17) except that normalization is such as to yield the spin-down rate of the vacuum rotator when $f_T = 1$. (18) has the same form as (14) if $n = .68, l = 0$, and $p = -1/2$ since $f_{\text{pc}} = R_A/R_L = (\Delta\theta_{\text{GEOM}}/\Delta\theta_{\text{CAP}})^2$. Also $A_1 = (4.4 \times 10^{12} \text{ G})^{-n} P_Q^{1-a} P_D^a$ with $a = e^{-\beta}$. Here $A_2 = \frac{3}{2} I c^3 / (2\pi)^2 R_*^6, I$ is the moment of inertia of the neutron star.

As a phenomenological way of accounting for f_T and $f_{\text{pc}} \neq 1$ we assume $f_T = f_0 P^m \dot{P}^k$ and $f_{\text{pc}} = f_1 P^q \dot{P}^r$ where f_0, f_1, m, k, q, r can be varied from their vacuum rotator values to isolate their effects on the cut-off line. As discussed earlier, the torque on neutron stars apparently decays on a time scale of 3×10^5 to 10^6 years. If it is due to alignment then $\sin i \propto e^{-t/\tau}$. If there is no alignment then $\tau \rightarrow \infty$, and $B_D \propto e^{-\gamma t}$.

With these assumptions the pair production cut-off line in the $P-\dot{P}$ diagram will be given by:

$$\begin{aligned} \dot{P}_{\text{crit}} &= [(2q+2r+1)\tau]^{E_3/E_1} A_1^{-2/E_1} A_2^{-n/E_1} f_1^{-4n/E_1} \\ &\times f_0^{-2p/E_1} (\sin i_0)^{(2n-2l)/E_1} P^{E_2/E_1} \\ &\text{for } P/\tau\dot{P} \gg 2q+2r+1 \\ &= A_1^{-2/E_4} A_2^{-n/E_4} f_1^{-4n/E_4} f_0^{-2p/E_4} (\sin i_0)^{(2n-2l)/E_4} P^{E_3/E_4} \\ &\text{for } P/\tau\dot{P} \ll 2q+2r+1, \quad (20) \end{aligned}$$

where $E_1 = 2pk + 4rl + l$, $E_2 = 2 + l - 2n - 4rn - 2pm - 4qn + 4rl$, $E_3 = 4rn + n - 4rl - l$, $E_4 = n + 2pk + 4rn$, and $E_5 = 2 - n - 4qn - 2pm$. If $E_1 = 0$, the cutoff line is vertical and

$$\begin{aligned} P_{\text{max}} &= A_1^{2/E_2} A_2^{n/E_2} f_1^{4n/E_2} f_0^{p/E_2} [\tau(2q+2r+1)]^{-E_3/E_2} \\ &\times [\sin i_0]^{(2l-2n)/E_2} \text{ for } P/\tau\dot{P} \gg 2q+2r+1. \end{aligned}$$

If $E_4 = 0$, the cutoff line is also vertical and

$$\begin{aligned} P_{\text{max}} &= A_1^{2/E_3} A_2^{n/E_3} f_1^{4n/E_3} f_0^{2p/E_3} [\sin i_0]^{(2l-2n)/E_3} \\ &\text{for } P/\tau\dot{P} \ll 2q+qr+1. \end{aligned}$$

Here we have made use of the fact that

$$\begin{aligned} \sin i &= \sin i_0 e^{-l/\tau} = \sin i_0 \tau^{(4r+1)/2} \\ &\times \dot{P}^{(4r+1)/2} \left[\frac{P}{2q+2r+1} + \tau\dot{P} \right]^{-(4r+1)/2} \end{aligned}$$

The braking index, $N = \Omega\dot{\Omega}/\dot{\Omega}^2$, can be written

$$N = 2 + \left(\frac{4q+1}{4r+1} \right) + \left(\frac{2}{4r+1} \right) \frac{P}{\dot{P}} \left(\frac{1}{\tau} + \gamma_d \right). \quad (21)$$

If it is assumed that $f_T = 1$, $f_{pc} = 1$, $\gamma_D = 0$, $\tau = \infty$, $\sin i \approx 1$, $I \sim 10^{45}$ g-cm², and $\beta \gtrsim 4$, the resulting cutoff line is given in Figure 7a. As is true of other pair creation models (Sturrock 1971; RS; AS), the line is shallower than the observed cutoff. Allowing for a distribution in mass and therefore in moment of inertia and surface field strength (Fujimura and Kennel 1980) smears out the cutoff but still does not match the slope or include all of the known pulsars. Allowing for a distribution in $\sin i_0$ results in a similar situation. We now proceed to identify the effects on the cutoff line of the relaxation of some of the above assumptions. From (13), we always have $n = 0.68$ and $p = -0.5$, since $\Delta\theta_{\text{cap}}/\Delta\theta_{\text{GEOM}} = f_{pc}^{-1/2}$.

$$a) f_T, f_{pc} \neq 1$$

Ignoring torque decay for the moment we can determine the f_T or f_{pc} required to match the observed cutoff line ($\dot{P} \sim 4.6 \times 10^{-17} P^5$), to equation (20). If the torque is reasonably given by the vacuum torque ($f_T =$

1), but we allow for departures in polar cap size, matching the slopes of the observed and theoretical lines requires $5k + m = 2.08$. If $k = 0$ (i.e., insensitivity to \dot{P}), $m = 2.08$ and $f_{pc} = 0.16 P^{2.1}$, thus requiring pulsars with periods less than 2.4 s to have substantially larger polar caps than expected from simple open field line models. If, on the other hand, $m = 0$ (insensitivity to P), then $k = 0.42$ and $f_{pc} = 0.55 \dot{P}_{15}^{0.42}$ (where $\dot{P}_{15} = \dot{P}/10^{-15}$), yielding values of f_{pc} of 0.08 at $\dot{P} = 10^{-17}$ to $f_{pc} = 3.8$ at $\dot{P} = 10^{-13}$. Thus a wider polar cap at low \dot{P} and a narrower one at large \dot{P} is required to match the data. However, if we assume $f_{pc} \equiv 1$, and adjust f_T , matching the slopes of the observed and theoretical lines requires $q + 5r = -0.76$. The braking index can also be used to constrain q and r if we assume that all pulsars have the same N . The only object with a well measured value of N is the Crab (Groth 1975), where $N \approx 2.5$. Since for the Crab $P/\dot{P} \ll \tau$, equation (18) yields $4q - 2r + 0.5 = 0$, so that $f_T = 1.6 P^{-0.18} \dot{P}_{15}^{-0.12}$ requiring an "effective torquing radius" slightly larger (smaller) than c/Ω at small (large) \dot{P} . If we now identify R_A with R_T , such that $f_{pc} = f_T = f$, using the same procedure as above we find that $f = 1.8 P^{-0.22} \dot{P}_{15}^{-0.20}$, which requires smaller polar caps than given by extrapolating the field lines from the light cylinder.

Notice that only small systematic perturbations of the model are required to achieve a correct line. It is fortunate that $f \sim 1$ is all that is needed because the following heuristic argument requires f to be on the order of unity: The magnetic field will be essentially dipolar in the regime $\beta R_* < r < f(c/\Omega)$ so that $(1) \rightarrow B \sim B_D(R_*/r)^3$. The set of open field lines will be determined by the requirement that the particle kinetic energy density not exceed the magnetic energy at the last closed field line. Thus $B^2(r = fc/\Omega)/8\pi \approx \eta_{R_*} \Delta\Phi B(r = fc/\Omega)/B_*$. Here $\Delta\Phi$ is the maximum available potential drop; from (9), $\Delta\Phi \sim f^{-1}(R_*\Omega/c)^2 B_D R$. Substituting for $B(r)$, η_{R_*} , and $\Delta\Omega$ require that $f^2 \sim 1$. This argument is equivalent to the detailed results of SAF, and applies either when pair creation is absent or when the potential drop at low altitude used to accelerate the primary beam and form pairs is of the order of the maximum potential, as is true in these models for pulsars near cutoff. An equivalent conclusion is reached when the induced B -field at the maximum radius of the last closed field line (due to current along open field lines) is compared with the dipole field (e.g., Scharlemann 1979). Then an induced toroidal field comparable to the dipole field at $r = fc/\Omega$ also requires $f \sim 1$.

Since pair creation in pulsars not near pair creation threshold probably reduces the available plasma energy density much below the maximum, a plausible physical interpretation of the ad hoc adjustment is $f_T = 1$ but $f_{pc} \neq 1$, since the geometry of current flow along B may depend on the magnetosphere structure, which may vary

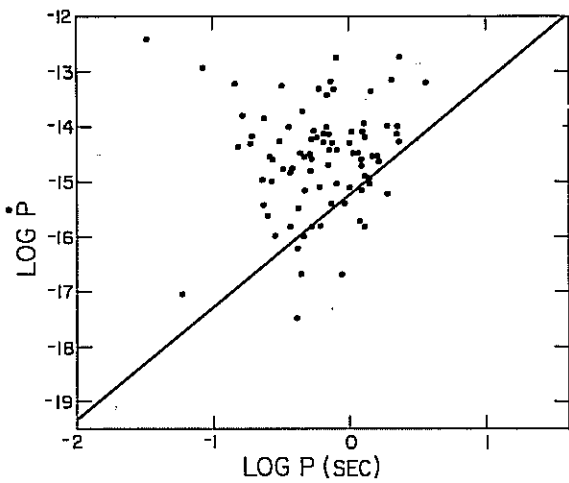


FIG. 7a

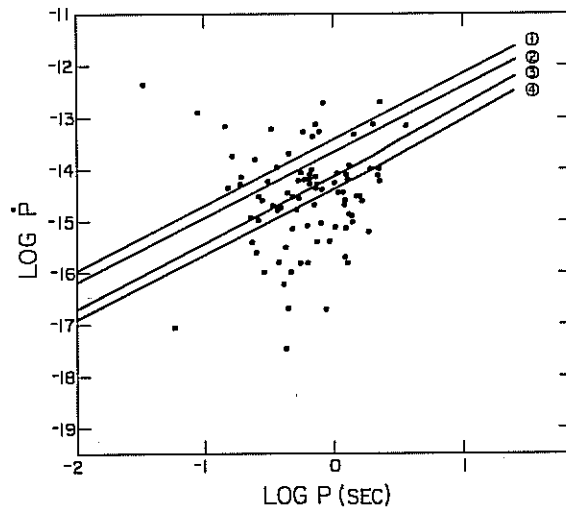


FIG. 7b

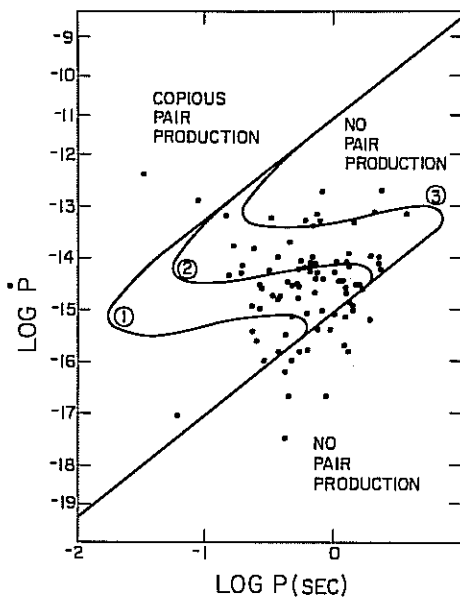


FIG. 7c

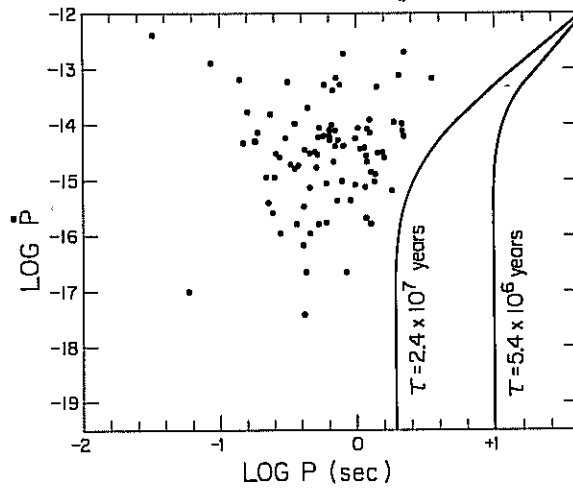


FIG. 7d

FIG. 7.—(a) The cutoff line in the P - \dot{P} diagram for pulsars with fields which are assumed to be static in strength and orientation in the rotating frame, and with moderately strong quadrupole component $\beta \approx 6$. (b) The cutoff line for decaying dipole and quadrupole components as discussed in § IVb. The initial quadrupole-dipole ratio is given by β_0 , and the dipole decay rate is given by γ . $\beta_0 = 4$ for lines 1 and 3, while $\beta_0 = 8$ for lines 2 and 4. $\gamma^{-1} = 3 \times 10^5$ years for lines 1 and 2 and $\gamma^{-1} = 3 \times 10^6$ years for lines 3 and 4. (c) The cutoff line for a growing quadrupole and decaying dipole, both on time scales of γ^{-1} , as discussed in § IVc. $\gamma^{-1} = 3 \times 10^6$, 1×10^6 , and 3×10^5 years for cutoff lines 1, 2, and 3, respectively. (d) The cutoff line for a constant β but with $\sin i$ exponentially decaying on a time scale, τ , as in § IVd. In this figure (as well as 7a, 7b, and 7c) $\sin i_0 = 1$ is assumed.

as the pulsar ages. An example of this effect occurs if Ω aligns with μ on the P/\dot{P} time scale. Then the area of the favorably curved flux tube *decreases* with age (assuming i_{QD} is small), since in the aligned (purely dipole) rotator no field lines are favorably curved. The sense of this alignment effect is the opposite of what is needed to explain the cutoff line in the $P-\dot{P}$ diagram as an effect of pair creation, and may have more to do with the dependence of pulse widths on age. Indeed, most evolutionary effects are not likely to lead to enlargement of the polar cap (relative to Goldreich and Julian's estimate) for small \dot{P} objects, which leads us to prefer the evolutionary effects discussed below, but the question of systematic departures of the area of the current flow tube from the conventional form, $\text{area} \propto P^{-1}$, for reasons other than alignment is quite open.

We now consider explicitly the effects on the cutoff line of models in which the torque decays on a time scale of $\sim 10^6$ years.

b) Dipole and Quadrupole Field Decay:

$$B_D = B_{D0} \exp(-\gamma_d t) \text{ and} \\ B_Q = B_{Q0} \exp(-3.33\gamma_d t)$$

In this scenario, A_1 of equation (18) is not a constant, but is given by equation (14) where $\beta = \beta(t) = \beta_0 \exp(-7\gamma_d t/3)$. Then $\beta = \beta_0 (B_D/B_{D0})^{7/3}$. It is easy to show that when $\sin i = \sin i_0$, $P \gg P_0$, and $f_{pc} = f_\tau \equiv f = f_0 P^m \dot{P}^k$,

$$\frac{B_D}{B_{D0}} = \left\{ \frac{1 + 2(k+m)\dot{P}}{\gamma_d P + [1 + 2(k+m)]\dot{P}} \right\}^{(1+4k)/2} \quad (22)$$

In (18) $A_1 = (4.4 \times 10^{12} \text{ gauss})^{-n} P_Q^{1-a} P_D^a$ with $a = e^{-\beta}$. Thus, the cutoff line is determined implicitly through equation (20). The parameters γ_d and β_0 are the important free parameters. Figure 7b shows examples of cutoff lines in this model when $f=1$. The slope is even shallower than in the nondecaying model, since at larger ages (small \dot{P}) the dipole field dominates, reducing the maximum period for pair creation and flattening the cutoff line. The combination of scenarios A and B then requires even more severe distortion (larger k and m) of the outer magnetosphere and polar cap size from the geometric estimate than is needed for nondecaying fields, in order to produce a slope in agreement with the data.

In this paper we considered only large scale (dipole and quadrupole) fields. Surface fields with spatial scales smaller than $\Delta R = R_* - R_{\text{CRUST}}$, corresponding to multipoles of order $l \gtrsim R_*/\Delta R$ decay on the crustal time scale $\gamma_c^{-1} \sim 3 \times 10^5 \sigma_{23} (1/l)^2$ years. Thus inclusion of higher order multipoles will not alter the slope substantially, since they will in general decay on an even more rapid time scale. Also, their addition will not substantially change the physics of pair production since the maximum available potential drops occur when $\rho \sim R_*$,

with further shortening of ρ hindering the global steady flow.

c) Magnetic Field Complication

We assume $B_D/B_{D0} = e^{-\gamma t}$ and $B_* = \text{constant}$, implying

$$\beta = e^{\gamma t} - 1 = \left\{ \frac{\gamma P + [1 + 2(k+m)\dot{P}]}{[1 + 2(k+m)]\dot{P}} \right\}^{(1+4k)/2} - 1.$$

Again A_1 is given by equation (14). Figure 7c shows the cutoff lines for this model, for various values of γ . It is clear that for large values of \dot{P} (young stars) the pure dipole line is obtained whereas for low \dot{P} (old stars) the large quadrupole plus moderate dipole line is approached.

The transition is accomplished with \dot{P}_{trans} determined by γ . For this model to be compatible with the observed distributions we must choose $\dot{P}_{\text{trans}} \gtrsim 10^{-12.5} \text{ s s}^{-1}$ or $\gamma^{-1} \lesssim 10^5$ years, in contradiction to the observed decay time of $\sim 10^6$ years. Physically, this indicates that if quadrupole growth occurs on the same time scale as dipole decay, then field line curvature does not occur soon enough in a pulsar's life to account for most pulsars. We point out, however, that the time scale for higher multipole growth may be shorter than the time scale for dipole decay; in our work here, we assumed these time scales to be the same. Clearly, quantitative models of this effect are of interest. Only if higher multipole growth times are longer than the dipole decay time scale will this scenario be in violation of the observed $P-\dot{P}$ distribution.

It has not escaped our attention that the upper cutoff line, $\dot{P} = \dot{P}_{\text{trans}1}$ may be used to explain the absence of pulsars with $\dot{P} > 10^{-12.5}$ if the time scale were short enough. However, the number of pulsars with high \dot{P} (shown in Fig. 7) is close to the number expected on the basis of time spent in that portion of the diagram, so no further explanation is needed. However, models of this type *predict* the absence of stars in the large \dot{P} region of the diagram, which may be testable as the number of stars with measured \dot{P} increases.

d) Alignment

Here $\sin i = \sin i_0 e^{-t/\tau}$, and, as discussed above, we assume the torque decays as $i \rightarrow 0$ in a manner similar to the vacuum rotator. When $t \gg \tau$, the first of equations (20) is relevant. $A_1 = (4.41 \times 10^{12} \text{ gauss})^{-n} P_D^a P_Q^{1-a}$ is assumed to be constant, typical of the complex field values of $\beta \approx 5$. The resulting cutoff line is illustrated in Figure 7d, in which $f=1$ and $P \gg P_0$ are assumed. The curve is easily understood. For large \dot{P} , $t/\tau \ll 1$ and alignment is negligible. Then the nonaligning, nondecaying cutoff line is appropriate. For $t/\tau \gg 1$, pulsars evolve on verti-

cal tracks with constant values of P , each vertical track obeying $P \propto B$. Since $P_{\max} \propto B^n$, a maximum period for pair creation exists independent of \dot{P} . This increases the area of the allowed region in the P - \dot{P} diagram, because a low value of \dot{P} implies a small value of i , not a weak field. This tends to increase the slope of the cutoff line in the P - \dot{P} diagram which is in the desired direction. However, the vacuum result that $P\dot{P} \propto \sin^2 i$ overcompensates and shifts a now vertical cutoff line to the right of the distribution of pulsars. Decreasing τ has the effect of causing a pulsar with a given magnetic field to evolve on an evolutionary curve which becomes vertical at a shorter period, thus long ($\sim 10^7$ years) decay times would be required to place the observed cutoff line near the observed population (cf. eq. [20], $E_4 = 0$).

e) Discussion

It is clear that slight modifications to the dipole plus quadrupole model without torque decay presented here would be sufficient to match the observed cutoff line (see § IVa). However, the evidence for torque decay is strong, and each of the theories presented has drawbacks tending to worsen agreement of the cutoff line with data. In the simple Cowling mode decay, it seems likely that higher multipole components will decay faster than the dipole component, even if the simple spherically uniform conductivity model fails in detail. If taken literally, this gives rise to a flatter cutoff line than is suggested by the data. However, it has been observed (cf. Phinney and Blandford 1980) that the number of pulsars per unit time interval decreases when the age is greater than one decay time (for $\tau \sim 10^6$ years), which is quite consistent with a wider distribution of initial β 's (i.e., multipole strengths) than assumed in Figure 7b. The cutoff "line" then is really only a line at large \dot{P} but becomes "fuzzy" for most of the lower half of the diagram, owing to the importance of the initial distribution of multipole components. The relative paucity of pulsars at low \dot{P} has also been ascribed to decrease in beaming angle if torque decay is due to alignment. If alignment occurs on the torque decay time scale, then the resulting cutoff line is well to the right of the observed distribution. Jones (1980) avoids this problem by assuming that at large ages $P\dot{P}$ reverts to a constant again due to the presence of a small residual torque due to small conduction currents in the aligned rotator, thus again shifting the line to the left and giving it a finite slope at low \dot{P} .

It is also possible that another criterion, such as the crossing of an instability threshold for the production of radio emission from the pair plasma or strong luminosity dependence on true age (cf. Ostriker and Gunn 1969; Manchester, private communication), would be required to explain the details of pulsar cutoff; the pair creation threshold is then an indirect criterion for the cessation of radio emission.

Alignment suffers from the absence of the directly observable consequence, that duty cycles of pulsars with small $\sin i$ should increase. If the opening angle of the beam also is proportional to $\sin i$, this objection would be unfounded, though it would be surprising if no strong luminosity variation with P/\dot{P} occurred. Recent results (Manchester, private communication) do suggest that the form of the observed cutoff line is dominated by luminosity evolution, for which alignment may be the most likely dynamical cause, since this can give rise to inhibition of the conduction currents whose flow is the basis of the radio emission (SAF; Arons 1981a; Michel and Pellat 1981). If luminosity evolution is the cause of the observed cutoff line, with luminosity and torque both decaying as the pulsar aligns, our model predicts faint pulsars to exist between the observed cutoff line and the lower branch of the pair creation cutoff line of Figure 7d.

The alternative decay theory of Flowers and Ruderman is not in agreement with the pair production hypothesis and the observed time scale for torque decay, if surface complexity arises strictly from secular MHD instability of the B -field with identical time scales for all components. Table 2 summarizes the favorable and difficult aspects of each torque decay model in the context of our steady flow model with a quadrupole component.

For completeness, we should also briefly review some possible reasons for the other borders in the P - \dot{P} diagram. For example, at large \dot{P} there is an absence of pulsars. If a torque decay time of $\sim 10^6$ years is assumed, then within statistical fluctuation the number of pulsars with ages less than 1 decay time (still short enough so that pair production cutoff effects are probably unimportant) is consistent with number of pulsars with ages less than 1/10 decay time, assuming there are equal numbers of pulsars in equal age intervals. Thus an upper limit to the magnetic field must exist. Various ideas have been advanced to account for this.

1. *Initial conditions.*—During neutron star formation the neutron star magnetic field is simply determined by the range in progenitor fields, with the assumption of flux freezing during the collapse.

2. *Shear strength of the crust (RS).*—In this interpretation RS showed that the crust shear stress cannot support the electromagnetic stress if $B_c \gtrsim 10^{13}$ gauss. If the large scale (poloidal) fields are supported by (toroidal) core currents, however, the vacuum field in the crust exerts no stress, and crustal shear strength limits only the departure from the vacuum B -field to values less than 10^{13} gauss. Thus, this argument only limits the magnitude of $l > R_*/\Delta R$ multipoles.

3. *Insufficient field line curvature at large P/\dot{P} .*—If the surface magnetic field starts out as a simple dipole and then becomes complicated later, the star can exist beyond the pure dipole cutoff line even for relatively small \dot{P} . This is illustrated in Figure 7c. It is a possibility

TABLE 2
SUMMARY OF EFFECTS OF TORQUE DECAY MODELS ON CUTOFF LINE AND P - \dot{P} DIAGRAM^a

| | Cowling Decay | MHD Complication | Alignment |
|--|--|---|--|
| Effect of cutoff line | Flatter than line with no decay | Has upper \dot{P} cutoff | Steeper than line with no decay |
| Favorable aspects | Explains torque decay; explains paucity of low \dot{P} pulsars as indicative of absence of higher multipole fields at large ages; crustal decay time similar to apparent torque decay time | Explains paucity of extreme high \dot{P} pulsars if $\gamma_Q^{-1} \sim 10^5$ yr (however, this is much shorter than observed torque decay time); explains torque decay; time scale of complication \sim crustal decay time $< 10^6$ yr | May explain torque decay; explains paucity of low \dot{P} pulsars as selection effect due to decreased emitting angle of beam |
| Theoretical difficulties in connection with pair production and observed cutoff line | Cutoff line too flat unless a large range of initial multipole moments is assumed | Torque decay requires $\gamma_D^{-1} \sim 10^7 \gamma_Q^{-1}$; asymptotic cutoff line too flat | Cutoff line too steep and too far to the right; requires an additional cutoff mechanism (e.g., plasma stability threshold, alterations of assumed torque from vacuum rotator or luminosity evolution |
| Other theoretical difficulties | Core conductivity suggests $\gamma_D^{-1} \gg 10^6$ years | Large uncertainty in actual decay modes | Vacuum torques align only when special conditions on ratio of internal toroidal to poloidal B -field conditions are met; expect distribution in τ ; plasma may change torque |
| Direct observational difficulties | ... | ... | Expect large duty cycle pulsars at low \dot{P} (not observed) unless opening angle of the beam also decreases with $\sin i$ |

^aApplied specifically to the model of this paper, but conclusions are qualitatively the same in general. See § III.

which is most pronounced in space-charge flow limited models (elaborated here in the electron emission case). Models with "vacuum" fields near the surface, as have been advocated for ion emission caps (RS; Jones 1978; Cheng and Ruderman 1980), have a pure dipole cutoff line closer to the curves appropriate to complex fields.

4. *Threshold for a plasma instability needed for coherence.*—A piece of evidence suggesting that (3) or (4) may be needed is that most of the known supernova remnants (~ 100) do not have pulsars associated with them, whereas as only two supernova remnants have associated pulsars (Phinney and Blandford 1980), a ratio not expected given the usual beaming angles of $\sim 15^\circ$ – 20° .

At low P and \dot{P} there also is an apparent absence of pulsars. Again initial conditions may account for the lower limit to the initial magnetic field strength, with the lower cutoff simply reflecting the evolutionary track of pulsars with the lowest field strength. It is again also possible that the criterion for a plasma instability has not been met. For example, if the relevant criterion is that the total energy in the gap between pair plasma and the walls of the flow tube exceed a minimum energy (Arons 1981a), then radio emission would cease for pulsars below and to the left of this line. The binary pulsar (PSR 1913+16) provides the single counterexample to the instability threshold hypothesis, however, since its evolutionary history has presumably been different (giving it a short period even with a weak field). Its radio pulse properties however must be determined only by its current physical conditions indicating that the region it occupies in the $P\dot{P}$ diagram is one in which radio emission can occur. The absence of pulsars in this region therefore is most likely attributable to the absence of stars having evolutionary paths through that region, or to luminosity evolution, as in the large P , small \dot{P} region.

V. POSSIBLE OBSERVATIONAL CONSEQUENCES OF SURFACE FIELD COMPLEXITY

A direct and unambiguous method for study of surface magnetic fields would be the observation of cyclotron absorption and scattering of soft X-ray photons in the low altitude field (AS; Arons 1979), emitted either by the heated polar caps or from other parts of the surface. If the region of radio emission, however, extends to within a radius $r \leq 2\beta R_* \lesssim 100$ km, some aspects of radio pulse morphology may be modified by such low altitude structure. In particular, separate pulse components ("interpulses") and/or pulses with large duty cycles may be formed because of the change in beaming direction with altitude. It is notable that if one *assumes* the existence of a radius to frequency map in the radio emission, such low altitudes may be required by the absence of aberration and time delay effects on the wave forms (Cordes 1978, 1981; Matese and Whitmire 1980).

Interpulses may arise from at least three sources: very wide hollow cones (Manchester and Lyne 1977), emission from opposite poles, and complex flux tubes from one pole. The three cases may be distinguishable by analysis of the polarization position angle as a function of longitude.

In the original idea of Radhakrishnan and Cooke (1969), the swing in position angle is due to a rotating vector (for example, the radius of curvature vector) as the line of sight samples different parts of the open flux tube. If this hypothesis is correct, then interpulses from the three different mechanisms will have different polarization swings. In a hollow cone the position angle swing should make one continuous curve, even though the intensity decreases between pulses. That is, one S shaped curve will result if i_0 , the angle between Ω and the observer, is close to i . If $|i_0 - i|$ is greater than a small fraction of the opening angle of the flux tube, the curve will appear more linear but still continuous. (Orthogonal mode transitions are assumed here to be transfer effects which can be transformed away to indicate the underlying structure [cf. Backer, Rankin, and Campbell 1976].

For orthogonal rotators, two S shaped or linear polarization swings can occur, having the property that the second pulse polarization swing will not be a simple extrapolation of the polarization sweep of the first pulse.

Low altitude emission beamed along B from $r < 2\beta R_*$ has quite different polarization and beaming properties. Because the whole flux tube curves, the observer's line of sight is tangent to B only for a narrow range of longitude *and* radius, and the magnetic field projected on the plane of the sky (or magnetic radius of curvature, or any other single rotating vector attached to the magnetic structure) is approximately constant throughout the exposure, instead of sweeping through a wide range of angles. Therefore, if the polarization is fixed by the magnetic structure alone, one expects a narrow pulse with an approximately fixed position angle through the wave form.

In rare special cases ($\alpha \approx \pi/2$), the observer's line of sight remains tangent to B at all r . Since the beaming direction changes drastically with respect to the dipole axis at radii less than $2\beta R_*$, the result would be a single large duty cycle wave form. A few pulsars do have wave forms of width greater than $\sim 70^\circ$, which have previously been interpreted as possibly due to radiation from the dipolar region but with small inclination angle i . Low altitude emission from strongly oblique but distorted fields provides an alternative geometric interpretation of these rare objects.

We point out that if low altitude emission from distorted geometries is relevant, then the emission of coherent radiation must be broad-band at each height, and cannot exhibit a radius to frequency map, for, if $\Delta\nu \ll \nu$ at each height and $\alpha \neq \pi/2$, the emission would

be seen as a single spectral line because of the change of basic beaming direction with height, in contrast to the essentially constant beaming direction in the dipolar zone. Since the actual spectra are broad-band, the emission in such low altitude models must be locally broad-band. The same requirement exists for the $\alpha \approx \pi/2$ case, since in no known example has strong spectral variation been observed as a function of longitude.

No observational or theoretical constraint presently known forbids broad-band emission. For example, if emission occurs only at one radius, local density and velocity gradients may give rise to widths which vary as a function of frequency even if the emission is narrow-band at each point in space. Thus widths which become narrower at high frequency may be due to gradients along the B -field (radius to frequency maps) or gradients across the B -field (single radius emission). The only constraint on the latter model is that the emission must be truly broad-band in each emitting element of plasma, or, if it is locally narrow-band, the angular width of the emission zone must be small compared to the longitude resolution of spectral observations.

We also point out that even if radius to frequency maps exist, surface multipoles are unlikely to explain the transition in the pulse separation versus frequency $W(\nu)$ curve. In many pulsars $W(\nu) \propto \nu^{-a}$, where $a \sim 0.2$, for ν less than ~ 1 GHz and $a \sim 0$ for $\nu > 1$ GHz (see Manchester and Taylor 1977; Bartel, Sieber, and Graham 1980 for summaries). As described above, the gross curvature of the flux tube at low altitude in general geometries will either present frequency dependence on longitude (not observed) or interpulse and/or large duty cycles if broad-band emission occurs. If the dipole and multipole axes are aligned, as in the "normal" pole of Appendix A, the problem of frequency shift with longitude is avoided since the tube does not bend. However, the $W(\nu)$ versus ν curves cannot be explained by appealing to higher multipoles. This can be illustrated as follows: Suppose narrow-band emission occurs at a local frequency $\nu \propto n^a$, where n is the particle density ($= e^\pm$ density in pair production models). Assume the plasma is uniform across B , and the plasma all streams outward relativistically along B , as in the bunched coherent curvature radiation models of Ruderman and Sutherland (1975) and of Benford and Buschauer (1977). Then $n/B = \text{constant}$ or $\nu \propto B^a$. For a pure multipole field of order l , this yields $\nu \propto r^{-(2+l)a}$, with $l=1$ for a dipole, $l=2$ for a quadrupole, etc. Since the flow zone is a flux tube, conservation of magnetic flux implies that the opening angle of a flux tube is proportional to $r^{-1}B^{-1/2} \propto r^{1/2}$ for a pure multipole. Then $\nu \propto W^{-2(1+2/l)a}$ where W = full width of the radiated beam, or $W \propto \nu^{-1/2(1+2/l)a}$. In the models referred to above, for example, $a = \frac{1}{2}$ since the radiated frequency is proportional to the local plasma frequency. However, in general, increasing the magnetic gradient ($l > 1$) makes

W a steeper, not a flatter, function of ν , contrary to most of the existing data.

Since the plasma streaming model has a number of restrictive assumptions, we think the more general argument comes from the fact that low altitude flux tubes have nondipolar bends, as well as nondipolar gradients, and that the change in the $W(\nu)$ function observed at high frequency is a consequence of changes in the radiative or refractive properties of the medium. Resolution of this issue requires a better ability to relate spectra and pulse shapes [from either low altitude ($r < 2\beta R_*$) or moderate altitude ($2\beta R_* < r < R_A$) regions] to the plasma conditions in these zones.

We therefore conclude that the observational identification of low altitude complexity in the magnetic field is hard to do from the radio data above; soft X-ray absorption would be much more direct. However, pulse components which do not show polarization sweep may be good candidates for such emission, and should be studied for other differences from more commonly observed components for clues to the physical differences between emission zones. The possibly observable effects of low altitude complexity on the P - \dot{P} diagram have been explored in § IV above.

VI. CONCLUSIONS

The main conclusions are the following:

1. Neutron stars with steady-state space charge limited flow in electron zones and with magnetic geometries including a dipole and quadrupole component will produce copious pairs, provided they satisfy the pair production threshold, equation (13). This can account for all pulsars if the ratio R_A/R_L or R_T/R_L are proportional to a small power in P or \dot{P} (as in § IVa), indicating physically small systematic departures of the outer magnetosphere from that of a vacuum rotator. We also note that a qualitative difference from the pure dipole field case occurs when $i=0$, where particle acceleration can exist if sufficient low altitude acceleration in the nondipole zone occurs.
2. The inclusion of torque decay in the simplest scenarios worsens the agreement of the cutoff line with the observed distribution, requiring larger departures in the outer magnetosphere from the vacuum rotator result. However, if alignment occurs, it is likely that pair production cessation does not directly account for the cutoff line; instead, luminosity evolution (Manchester, private communication) or another physical cutoff criterion is required. If luminosity evolution occurs with torque decay, then faint (and thus difficult to detect) pulsars would be expected in the lower right edge of the diagram.
3. Observational effects of the higher order fields may be difficult to detect directly, but in some cases

they may account for interulses or long duty cycles, and should have identifiable polarization patterns. The flattening at high frequency of the observed relation between pulse width and frequency, however, cannot be easily accounted for by appealing to higher order multipole components.

This work was supported by NSF grants AST 79-23243 and AST 78-17242, by the John Simon Guggenheim Foundation, and by the taxpayers of the State of California. We are indebted to C. F. McKee for encouraging conversations and to the referee for useful comments.

APPENDIX A

ALIGNED QUADRUPOLE AND DIPOLE AXES

When $i_{QD} = 0$, the magnetic field structure is axisymmetric. Then $\mathbf{B} = \nabla \times (A \mathbf{e}_\phi)$, where \mathbf{e}_ϕ is the unit vector in the toroidal direction with respect to the magnetic axis. The quantity $2\pi r \sin \theta A(r, \theta)$ is the magnetic flux passing through a circle of radius $r \sin \theta$ centered on the magnetic axis and passing through the point (r, θ) , and so $r \sin \theta A = \text{constant}$ along a field line. In this geometry

$$B_r = B_D \left[\frac{\cos \theta}{x^3} + \frac{1}{2} \beta \frac{(3 \cos^2 \theta - 1)}{x^4} \right] \quad (\text{A1})$$

and

$$B_\theta = B_D \left(\frac{\sin \theta}{2x^3} + \beta \frac{\cos \theta \sin \theta}{x^4} \right), \quad (\text{A2})$$

where $x = r/R_*$, $\theta = \text{magnetic colatitude}$, and $\beta = B_Q/B_D$ is the ratio of polar magnetic field strengths. Then:

$$A = B_D R_* \frac{\sin \theta}{2x^2} + \frac{B_Q R \cos \theta \sin \theta}{2x^3}. \quad (\text{A3})$$

From the constancy of flux along a field line we find:

$$\frac{r(\theta)}{R_*} = \frac{1}{2} (1 + \beta \cos \theta_*)^{-1} \left\{ \frac{\sin^2 \theta}{\sin^2 \theta_*} \pm \left[\left(\frac{\sin \theta}{\sin \theta_*} \right)^4 + 4(1 + \beta \cos \theta_*) \beta \cos \theta \left(\frac{\sin \theta}{\sin \theta_*} \right)^2 \right]^{1/2} \right\}. \quad (\text{A4})$$

Figure 8 shows the global structure of this magnetic field. As can be seen from the figure, in the region where the dipole field merges with the quadrupole field of opposite polarity, the radius of curvature can be small [$\rho(r=R_*) \approx \beta R_*/2$ when $\beta \geq 1$]. In this case, the "polar flux tube" is a thin cylindrical shell at altitudes below the neutral point, $r/R_* < \beta$, $\pi/2 < \cos^{-1}(-1/\beta) \leq \theta \leq \pi$. The polar boundary of this acceleration zone is located along the flux surface

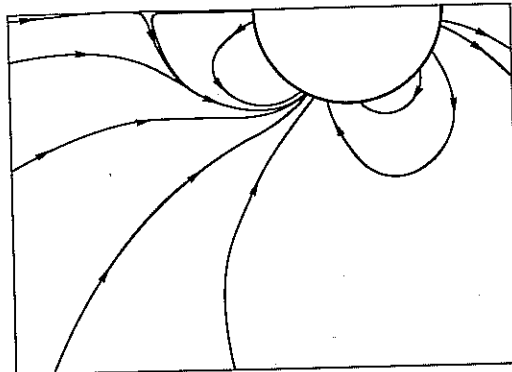


FIG. 8.—Aligned dipole and quadrupole. The global field line structure of an aligned ($i_{QD} = 0$) quadrupole and dipole with $\beta = 2$, as represented by eq. (A4).

$\theta_* = \cos^{-1}(-1/\beta)$. Field lines lying close to this boundary are described by:

$$\frac{r}{R_*} \approx -\beta \cos \theta + (\beta^2 - 1)^{3/2} \Delta\theta_* \cot^2 \theta, \quad (\text{A5})$$

where

$$\Delta\theta_* = \theta_* - \cos^{-1}(-1/\beta). \quad (\text{A6})$$

Tracing the field lines back to R_A with the field approximately dipolar for $r \gg R_*\beta$ gives an angular width of the acceleration zone:

$$\Delta\theta_c = \frac{\beta^2}{(\beta^2 - 1)^{3/2}} \left(\frac{R_*\Omega}{c} \right) \left(\frac{R_L}{R_A} \right). \quad (\text{A7})$$

Because the "polar" flux is concentrated in a belt rather than a tube, the smallest dimension is $\sim R_*(R_*\Omega/c)(R_L/R_A)$, much smaller than the size typical of standard polar cap models [where $\Delta\theta_c \sim (R_*\Omega/c)^{1/2}(R_L/R_A)^{1/2}$].

The electric potential in this geometry is not given by (9). Instead a one-dimensional approximation is appropriate at $r \ll \beta R_*$. Consider a point on the flux surface $\theta_* = \cos^{-1}(-1/\beta) = \theta_m$ at a distance s along the field line from the stellar surface. Erect a normal to this surface pointing into the acceleration zone. Let x = the distance along this normal. Then:

$$\Phi \approx -2\pi \left[\eta(\theta_* = \theta_m, s) - \eta_R(\theta_* = \theta_m, s) \right] (x^2 - xx_{\max}). \quad (\text{A8})$$

We find x and x_{\max} by using (A5) to note that an increment in magnetic colatitude $\delta\Delta\theta_*$ across the open flux lines corresponds to an increment in radius, Δr , such that

$$\Delta r = R_*(\beta^2 - 1)^{3/2} \delta\Delta\theta_* \cot^2 \theta, \quad (\text{A9})$$

while from flux conservation,

$$x = B_\theta \Delta r / B. \quad (\text{A10})$$

The quantity x_{\max} is obtained by setting $\Delta\theta_*$ equal to $\Delta\theta_c$ of (A7). We consider only the case $i=0$. Although this case has unfavorably curved field lines for $r \gg \beta R_*$, it illustrates the potential drops available in the near region.

Calculation of the charge density requires a knowledge of the component of B parallel to Ω_* . In the low-altitude acceleration region where $r \approx -R_*\beta \cos \theta$ we find:

$$\eta - \eta_R = \frac{-\Omega B_D}{2\pi c} \left[\frac{(\beta^2 - 1)^{1/2}}{\beta^5} \frac{\sin \theta}{\cos^4 \theta} + \frac{1}{\beta^3} \frac{\sin^2 \theta}{\cos^3 \theta} \right]. \quad (\text{A11})$$

Use of (A11), (A10), and (A9) calculated at the center of the flow region $\Delta\theta_* = \Delta\theta_{c/2}$ in (A8) yields

$$\Phi = \frac{1}{4} B_D R_* \left(\frac{R\Omega}{c} \right)^3 \left(\frac{R_L}{R_A} \right)^3 \left[\frac{-(\beta^2 - 1)^{1/2} \cos^2 \theta}{\beta} \frac{\sin^2 \theta}{\sin^2 \theta} + \frac{\beta |\cos^3 \theta|}{\sin^2 \theta} \right]. \quad (\text{A12})$$

In order to find the optical depth, we adopt the "on the spot" approximation, in which the magnitude of B is assumed constant along the ray between emission and absorption points, and the pitch angle of the photon is $\Psi = l/\rho$ where l is the length traveled by the photon (AS). Then

$$\tau = 0.086 \frac{\alpha_F}{\lambda_c} \left(\frac{B}{B_q} \right)^2 \frac{\epsilon}{m_e c^2} \rho \Psi^3 \exp \left(\frac{-8}{3} \frac{B_q}{B \Psi} \frac{m c^2}{\epsilon} \right). \quad (\text{A13})$$

The optical depth τ is then maximized when Ψ has the maximum value possible achieved just as a photon leaves the acceleration zone. Then $\Psi_{\max} \approx (x_{\max}/\rho)^{1/2}$, and with $\epsilon \approx \epsilon_c$ and Φ given by (A12) we find the maximum τ as a function of θ (and implicitly as a function of emission altitude),

$$\begin{aligned} \tau_{\max}(\theta) = & 1.5 \times 10^{39} \left(\frac{B_D}{4.4 \times 10^{12} \text{ G}} \right)^5 \left(\frac{R_*}{10 \text{ km}} \right)^3 \beta^{-9/2} \left(\frac{R_* \Omega}{c} \right)^{21/2} \left(\frac{R_L}{R_A} \right)^{15/2} \frac{|\cos \theta|^{5/2}}{(\sin \theta)^7} \left[\beta |\cos \theta| - \frac{\sqrt{\beta^2 - 1}}{\beta \sin \theta} \right]^3 \\ & \times \exp \left[-8.13 \times 10^{-28} \beta^{7/2} \left(\frac{R_* \Omega}{c} \right)^{-19/2} \left(\frac{R_A}{R_L} \right)^{13/2} \left(\frac{4.4 \times 10^{12}}{B_D} \right)^4 \left(\frac{10 \text{ km}}{R_*} \right)^2 \frac{\sin^6 \theta}{|\cos \theta|^{7/2}} \left(\beta |\cos \theta| - \frac{\sqrt{\beta^2 - 1}}{\beta \sin \theta} \right)^{-3} \right]. \end{aligned} \quad (\text{A14})$$

For fixed β , we maximize $\tau_{\max}(\theta)$ with respect to θ . This maximum exists since at the surface, where B is strong and ρ is small, Φ is small and therefore the photon energy ϵ is small, yielding a small τ_{\max} , while at higher altitude the neutral point at $r = \beta R_*$, $\theta = \pi$, is approached so that B can be weak and Φ may again be small, depending on whether the field lines are favorably curved. The maximum of τ_{\max} occurs as

$$\theta \approx \pi - \frac{1}{2} \sin^{-1} \left[\frac{3(\beta^2 - 1)^{1/2}}{\beta^2} \right] \quad (\text{A15})$$

which yields:

$$\begin{aligned} (\tau_{\max})_{\max} = & 7.43 \times 10^{-3} \left(\frac{B_D}{4.4 \times 10^{12} \text{ G}} \right)^5 \left(\frac{R_*}{10 \text{ km}} \right)^{27/2} \beta^{11/2} P^{-21/2} \left(\frac{R_L}{R_A} \right)^{15/2} \nu \\ & \times \exp \left[-2.23 \times 10^{10} \left(\frac{B_D}{4.4 \times 10^{12} \text{ G}} \right)^{-4} \left(\frac{10 \text{ km}}{R_*} \right)^{23/2} \beta^{-11/2} \nu^{-1} P^{19/2} \left(\frac{R_A}{R_L} \right)^{13/2} \right], \end{aligned} \quad (\text{A16})$$

where $\nu = \bar{\epsilon}/\epsilon_c$ (typically $\bar{\epsilon}$, the mean photon energy that is absorbed at $\tau \approx 1$, is $\sim 2\epsilon_c$).

For sufficiently small P , $(\tau_{\max})_{\max} \gg 1$, indicating copious pair production. We find the maximum period by setting $(\tau_{\max})_{\max} = 1$ and solve for the period to find

$$P_{\max} = 0.511 \left(\frac{B_D}{4.417 \text{ G}} \right)^{8/19} \left(\frac{R_*}{10 \text{ km}} \right)^{23/19} \beta^{11/19} \nu^{2/19} \left[\frac{\ln \Lambda}{18.23} \right]^{2/19} \quad (\text{A17})$$

with

$$\ln \Lambda = 18.23 + \ln \left[\left(\frac{0.11 \text{ s}}{P} \right) \nu \beta^{11/2} \left(\frac{R_*}{10 \text{ km}} \right)^{27/2} \left(\frac{B_D}{4.4 \times 10^{12} \text{ G}} \right)^5 \left(\frac{R_L}{R_A} \right)^{-15/2} \right]. \quad (\text{A18})$$

Clearly for $1 < \beta < 10$ (the range where the model is self-consistent and where ρ is interestingly small), $P_{\max} < 0.4 \text{ s}$ for all reasonable values of B_0 and R_* . Thus, the axisymmetric model does not yield a sufficiently large maximum period for pair creation, in spite of small radius of curvature. The reason for this failure is twofold. The geometry of the thin strip for the acceleration zone, instead of a more or less round tube, reduces the potential by a factor $\sim (R_* \Omega/c)^{1/2}$ compared to the dipole potential. Second, as r approaches βR_* the geometry is not so thin, but the field line curvature is no longer favorable and the presence of the neutral point in B reduces the opacity, since $|B|$ is smaller. The main point of this axisymmetric model is to show that short radius of curvature *alone* will not guarantee pair formation, since the potential is also affected and since maintenance of consistently favorable curvature does not always occur.

APPENDIX B

ANALYTIC SOLUTION FOR FIELD LINES FOR $x \sin \psi \gg \beta$

$$B_r = \frac{B_D}{x^3} \left\{ \cos \psi + \frac{3\beta \cos [2(\psi - i_{QD})] + 1}{4x} \right\}, \tag{B1}$$

$$B_\psi = \frac{B_D}{x^3} \left\{ \frac{\sin \psi}{2} + \frac{\beta \sin [2(\psi - i_{QD})]}{2x} \right\}. \tag{B2}$$

If $x \sin \psi \gg \beta$, then

$$\frac{dx}{d\psi} \approx x \left[\frac{2 \cos \psi}{\sin \psi} + \beta \left\{ \frac{3 \cos [2(\psi - i_{QD})] + 1}{2x \sin \psi} \right\} \left[1 - \frac{\beta \sin (2\psi - 2i_{QD})}{x \sin \psi} \right] \right]. \tag{B3}$$

Keeping terms of order x and 1, eliminating terms of order $1/x$ yields

$$\frac{dx}{d\psi} = \frac{2x \cos \psi}{\sin \psi} + \beta \left[\frac{[3 \cos (2\psi - 2i_{QD}) + 1]}{4 \sin \psi} - \frac{2 \sin (2\psi - 2i_{QD}) \cos \psi}{\sin^2 \psi} \right].$$

Let

$$f(\psi) = 2 \cot \psi \text{ and } g(\psi) = \beta \left[\frac{3 \cos (2\psi - 2i_{QD}) + 1}{4 \sin \psi} - \frac{2 \sin (2\psi - 2i_{QD}) \cos \psi}{\sin^2 \psi} \right].$$

Then the solution of the linear first order differential equation is:

$$x = \exp \left[\int^\psi f(\psi') d\psi' \right] \int g(\psi) \exp \left[- \int^\psi f(\psi') d\psi' \right] d\psi + C \exp \left[\int f(\psi) d\psi \right],$$

where C is an integration constant.

Performing the integrations yields:

$$x = C \sin^2 \psi + \beta \sin^2 \psi \left[\left(\frac{5C_1 - 1}{4} \right) \frac{\cos \psi}{\sin^2 \psi} + \left(\frac{1 - C_1}{4} \right) \ln \left| \frac{1}{\sin \psi} - \frac{\cos \psi}{\sin \psi} \right| + S_1 \left(\frac{1}{3 \sin^2 \psi} - \frac{5}{\sin \psi} \right) \right].$$

Here, $C_1 = \cos 2i_{QD}$ and $S_1 = \sin 2i_{QD}$. Thus, the two field lines which pass through the point $x = c/R_*\Omega$, $\psi = \pm \pi/2$, are given by:

$$x = \sin^2 \psi \left\{ \frac{c}{R_*\Omega} \pm \frac{14}{3} \beta S_1 + \beta \left[\left(\frac{5C_1 - 1}{4} \right) \frac{\cos \psi}{\sin^2 \psi} + \left(\frac{1 - C_1}{4} \right) \ln \left| \frac{1 - \cos \psi}{\sin \psi} \right| + S_1 \left(\frac{1}{3 \sin^2 \psi} - \frac{5}{\sin \psi} \right) \right] \right\}. \tag{B4}$$

This solution approaches the form $x = (c/R_*\Omega) \sin^2 \psi + \beta \cos \psi$ for $i_{QD} = 0$, which is also the asymptotic form for the exact analytic solution (eq. [A4]) in the limit of large x .

REFERENCES

Arons, J. 1979, *Space Sci. Rev.*, **24**, 437.
 ———. 1981a, in *IAU Symposium 95, Pulsars*, ed. W. Sieber and P. Wielebinski (Dordrecht: Reidel), p. 69.
 ———. 1981b, *Ap. J.*, **248**, 1099.
 ———. 1981c, in *IAU Symposium 94, Origin of Cosmic Rays*, ed. G. Setti, G. Spada, and A. Wolfendale (Dordrecht: Reidel), p. 175.
 Arons, J., and Scharlemann, E. T. 1979, *Ap. J.*, **231**, 854 (AS).
 Backer, D. C. 1976, *Ap. J.*, **209**, 895.
 Backer, D. C., Rankin, J. M., and Campbell, D. B. 1976, *Nature*, **236**, 202.
 Backus, G. 1956, *Ap. J.*, **123**, 508.
 Bartel, N., Sieber, W., and Graham, D. A. 1980, *Astr. Ap.*, **87**, 282.

- Baym, G., Pethick, C., and Sutherland, P. G. 1971, *Ap. J.*, **170**, 299.
- Benford, G. 1977, *M.N.R.A.S.*, **179**, 311.
- Benford, G., and Buschauer, R. 1977, *M.N.R.A.S.*, **178**, 189.
- Cheng, A. F., and Ruderman, M. A. 1977, *Ap. J.*, **214**, 598.
- _____. 1980, *Ap. J.*, **235**, 576.
- Cordes, J. M. 1978, *Ap. J.*, **222**, 1006.
- _____. 1981, in *IAU Symposium 95, Pulsars*, ed. W. Sieber and R. Wielebinski (Dordrecht: Reidel), in press.
- Davis, L., and Goldstein, M. 1970, *Ap. J. (Letters)*, **159**, L81.
- Erber, T. 1966, *Rev. Mod. Phys.*, **38**, 620.
- Fawley, W. M. 1978, Ph.D. dissertation, University of California, Berkeley.
- Fawley, W. M., Arons, J., and Scharlemann, E. T. 1977, *Ap. J.*, **217**, 227 (FAS).
- Flowers, E. G., and Ruderman, M. A. 1977, *Ap. J.*, **215**, 302.
- Fujimura, F. S. and Kennel, C. F. 1980, *Ap. J.*, **236**, 245.
- Goldreich, P. 1969, *Proc. Astr. Soc. Australia*, **1**, 227.
- _____. 1970, *Ap. J. (Letters)*, **160**, L11.
- Goldreich, P., and Julian, W. H. 1969, *Ap. J.*, **157**, 869.
- Goldreich, P., Pacini, F., and Rees, M. J. 1971, *Comments Ap. Space Phys.*, **3**, 185.
- Groth, E. J. 1975, *Ap. J. Suppl.*, **29**, 431.
- Gunn, J. E., and Ostriker, J. P. 1969, *Nature*, **221**, 454.
- _____. 1970, *Ap. J.*, **160**, 979.
- Harding, A. K. 1981, preprint.
- Holloway, N. J. 1975, *M.N.R.A.S.*, **171**, 619.
- Jackson, E. A. 1976, *Ap. J.*, **206**, 831.
- Jones, P. B. 1976, *Nature*, **262**, 120.
- _____. 1977, *Nature*, **270**, 37.
- _____. 1978, *M.N.R.A.S.*, **184**, 807.
- _____. 1979, *Ap. J.*, **228**, 536.
- _____. 1980, *Ap. J.*, **237**, 590.
- Kennel, C. 1979, in *Particle Acceleration Mechanisms in Astrophysics*, ed. J. Arons, C. Max, and C. McKee (New York: American Institute of Physics), p. 391.
- Lamb, H. 1883, *Phil. Trans.*, **174**, 519.
- Lyne, A. G., Ritchings, R. T., and Smith, F. G. 1975, *M.N.R.A.S.*, **171**, 579 (LRS).
- Macy, W. W., Jr. 1974, *Ap. J.*, **190**, 153.
- Manchester, R. N., and Lyne, A. G. 1977, *M.N.R.A.S.*, **181**, 761.
- Manchester, R. N., and Taylor, J. H. 1977, *Pulsars* (San Francisco: Freeman).
- Markey, P., and Tayler, R. J. 1973, *M.N.R.A.S.*, **163**, 77.
- Matese, J. J., and Whitmire, D. P. 1980, *Ap. J.*, **235**, 587.
- Mestel, L. 1971, *Nature Phys. Sci.*, **233**, 149.
- Michel, F. C. 1975, *Ap. J.*, **197**, 193.
- _____. 1979, *Ap. J.*, **227**, 579.
- Michel, F. C., and Goldwire, H. C. 1970, *Ap. Letters*, **5**, 21.
- Michel, F. C., and Pellat, R. 1981, in *IAU Symposium 95, Pulsars*, ed. W. Sieber and P. Wielebinski (Dordrecht: Reidel), p. 37.
- Okamoto, I. 1974, *M.N.R.A.S.*, **167**, 457.
- Ostriker, J. P., and Gunn, J. E. 1969, *Nature*, **227**, 813.
- Phinney, E. S., and Blandford, R. D. 1981, *M.N.R.A.S.*, **194**, 137.
- Radhakrishnan, V., and Cooke, D. J. 1969, *Ap. Letters*, **3**, 225.
- Roberts, D. H., and Sturrock, P. A. 1972, *Ap. J.*, **222**, 297.
- Ruderman, M. A., and Sutherland, P. A. 1972, *Ap. J.*, **196**, 51 (RS).
- Rylov, Y. A. 1979, *Ap. Space Sci.*, **66**, 401.
- Scharlemann, E. T. 1979, in *Particle Acceleration Mechanisms in Astrophysics*, ed. J. Arons, C. E. Max, and C. F. McKee (New York: American Institute of Physics), p. 373.
- Scharlemann, E. T., Arons, J., and Fawley, W. M. 1978, *Ap. J.*, **222**, 297 (SAF).
- Sturrock, P. 1970, *Nature*, **227**, 465.
- _____. 1971, *Ap. J.*, **164**, 529.
- Tademaru, E. 1974, *Ap. Space Sci.*, **30**, 179.
- Tsai, W., and Erber, T. 1974, *Phys. Rev. D*, **10**, 492.

JOHN J. BARNARD and JONATHAN ARONS: Astronomy Department, 601 Campbell Hall, University of California, Berkeley, CA 94720